Wiener path integrals and multi-dimensional global bases for non-stationary stochastic response determination of structural systems

Apostolos F. Psaros, Ioannis Petromichelakis, Ioannis A. Kougioumtzoglou *

Department of Civil Engineering and Engineering Mechanics, Columbia University, 500 W 120th St, New York, NY 10027, United States

ARTICLE INFO

ABSTRACT

A novel approximate technique based on Wiener path integrals (WPIs) is developed for determining, in a computationally efficient manner, the non-stationary joint response probability density function (PDF) of nonlinear multi-degree-of-freedom dynamical systems. Specifically, appropriate multi-dimensional (time-dependent) global bases are constructed for approximating the non-stationary joint response PDF. In this regard, two distinct approaches are pursued. The first employs expansions based on Kronecker products of bases (e.g., wavelets), while the second utilizes representations based on positive definite functions. Next, the localization capabilities of the WPI technique are exploited for determining PDF points in the joint space-time domain to be used for evaluating the expansion coefficients at a relatively low computational cost. In contrast to earlier implementations of the WPI technique, the herein developed generalization and enhancement circumvents computationally daunting brute-force discretizations of the time domain in cases where the objective is to determine the complete time-dependent non-stationary response PDF. Several numerical examples pertaining to diverse structural systems are considered, including both single- and multi-degree-of-freedom nonlinear dynamical systems subject to non-stationary excitations, as well as a bending beam with a non-Gaussian and non-homogeneous Young's modulus. Comparisons with pertinent Monte Carlo simulation data demonstrate the accuracy of the technique.

© 2019 Elsevier Ltd. All rights reserved.

1. Introduction

Problems involving a probabilistic description of excitation and media properties occur in abundance in engineering (e.g., [1,2]). Clearly, this increased sophistication in modeling, in conjunction with complex nonlinear behaviors, renders the response analysis of many engineering systems a challenging task. In this regard, there is a wide range of solution techniques developed over the past few decades in the field of stochastic engineering dynamics and mechanics (e.g., [3–9]). Nevertheless, solving in a computationally efficient manner high-dimensional nonlinear stochastic differential equations (SDEs) modeling the system dynamics remains a persistent challenge.

Recently, a promising technique has been developed for determining the stochastic response of nonlinear multi-degree-of-freedom (MDOF) systems, which relates to the concept of the Wiener path integral (WPI) [10,11]. The notion of

---

* Corresponding author.
E-mail address: ikougioum@columbia.edu (I.A. Kougioumtzoglou).

path integral, which generalizes integral calculus to functionals, was introduced by Wiener [12] and by Feynman [13], independently, and has been an instrumental mathematical tool in the field of theoretical physics [14]. It is noted that the WPI based technique developed by Kougioumtzoglou and co-workers exhibits significant versatility and can account even for systems endowed with fractional derivative terms [15]. Furthermore, it has been extended for addressing certain one-dimensional mechanics problems with random material/media properties [16], systems subject to non-white and non-Gaussian stochastic processes [17], as well as a class of nonlinear electromechanical energy harvesters [18].

From a computational efficiency perspective, recent work by Kougioumtzoglou et al. [19] and by Psaros et al. [20] has reduced drastically the computational cost of the standard numerical implementation of the technique by resorting to sparse representations of the joint response probability density function (PDF) in conjunction with compressive sampling schemes. Nevertheless, the above developments and implementations rely on time-invariant joint response PDF expansions, or in other words, the objective is to determine the joint response PDF at a specific time instant. Although this localization capability can be considered as an advantage of the technique (for instance, the stationary response PDF can be determined directly at a reduced cost, without necessarily obtaining the global solution first), in many cases the determination of the complete time-dependent non-stationary joint response PDF is required (e.g., cases of evolutionary excitations [21]). Addressing this challenge by discretizing the temporal dimension in a brute-force manner and applying the technique for each and every time instant would render the numerical implementation computationally daunting. In this regard, the objective of this paper relates to generalizing the WPI technique and further enhancing its computational efficiency by constructing time-dependent bases for determining the non-stationary response PDF directly, based on knowledge of relatively few PDF points in the joint space-time domain.

Evaluating the PDF of a stochastic process given partial information is a typical problem in a wide range of research fields [22,23]. In stochastic dynamics PDF expansions have been utilized for solving the Fokker-Planck (FPE) and the Backward Kolmogorov (BKE) equations [24,25], or other alternative equations governing the stochastic response of a dynamical system [26]. Indicatively, PDF expansions have been coupled with weighted residual methodologies [27–30], where the approximate PDF is substituted into the FPE and the residual error is minimized; with moment closure schemes [31–35], which yield a finite set of moment equations to be solved for approximating the response PDF; with finite element method direct numerical solution schemes [36,37]; with discretized Chapman-Kolmogorov equation schemes propagating the response PDF in short time steps [38–41]; and with solution schemes based on the maximum entropy principle [42,43]. Typical PDF expansions and approximation schemes utilize truncated Gram-Charlier or Edgeworth series [31,32,25,27,30], Hermite or other polynomials [33,29,36,44,41,35], Gaussian distributions with varying mean and variance [45], kernel density functions [26] and B-splines or piecewise linear functions [38,40]. Further, McWilliam et al. [28] employed Shannon wavelets for approximating the PDF within the context of the weighted residual method. Moreover, radial basis functions (RBFs) demonstrated accurate results in the context of numerically solving the FPE [46,47].

In this paper an approximation scheme based on the WPI technique is developed for efficiently determining the non-stationary joint response PDF of stochastically excited MDOF dynamical systems. To this aim, two distinct expansions are proposed for the PDF; the first is based on Kronecker products of bases such as wavelets, and the second is based on positive definite functions, which is a more general class of functions than RBFs. As a result, the WPI technique is generalized herein to account explicitly for the time dimension in its formulation and implementation. The paper is organized as follows: in Section 2 the mathematical formulation of the WPI technique is outlined, in Section 3 various approximation schemes are developed, and in Section 4 three illustrative numerical examples demonstrate the reliability of the proposed technique.

2. Wiener Path Integral technique

In this section, the main theoretical and numerical aspects of the WPI technique are delineated for completeness. A more detailed presentation can be found in [17].

2.1. Wiener Path Integral formalism

In general, a wide range of problems in engineering mechanics and dynamics can be described by stochastic equations of the form

$$\boldsymbol{F}[\boldsymbol{x}] = \boldsymbol{f} \tag{1}$$

where $\boldsymbol{F}[.]$ represents an arbitrary nonlinear differential operator; $\boldsymbol{f}$ denotes the external excitation; and $\boldsymbol{x}$ is the system response to be determined. In the following, an MDOF nonlinear dynamical system with stochastic external excitation is considered in the form

$$\boldsymbol{M}\ddot{\boldsymbol{x}} + \boldsymbol{C}\dot{\boldsymbol{x}} + \boldsymbol{K}\boldsymbol{x} + \boldsymbol{g}(\boldsymbol{x}, \dot{\boldsymbol{x}}) = \boldsymbol{f}(t) \tag{2}$$

where $\boldsymbol{x}$ is the displacement vector process ($\boldsymbol{x} = [x_1, \ldots, x_m]^T$); $\boldsymbol{M}, \boldsymbol{C}, \boldsymbol{K}$ correspond to the $m \times m$ mass, damping and stiffness matrices, respectively; $\boldsymbol{g}(\boldsymbol{x}, \dot{\boldsymbol{x}})$ denotes an arbitrary nonlinear vector function; and $\boldsymbol{f}(t)$ is, in general, a non-stationary, non-white, and non-Gaussian vector process expressed as [4,5]

$$\boldsymbol{f}(t) = \boldsymbol{D}(t)\xi(t) \tag{3}$$

where $\boldsymbol{D}(t)$ is a diagonal matrix of deterministic time-modulating functions $d_j(t)$, $j \in \{1, \ldots, m\}$, and $\boldsymbol{\xi}(t)$ is given as the response of the nonlinear filter equation

$$\boldsymbol{P}\ddot{\boldsymbol{\xi}} + \boldsymbol{Q}\dot{\boldsymbol{\xi}} + \boldsymbol{R}\boldsymbol{\xi} + \boldsymbol{u}(\boldsymbol{\xi}, \dot{\boldsymbol{\xi}}) = \boldsymbol{w}(t) \tag{4}$$

where $\boldsymbol{P}, \boldsymbol{Q}, \boldsymbol{R}$ denote coefficient matrices; $\boldsymbol{u}(\boldsymbol{\xi}, \dot{\boldsymbol{\xi}})$ is an arbitrary nonlinear vector function; and $\boldsymbol{w}(t) = [w_1, \ldots, w_m]^T$ is a white noise stochastic vector process with the power spectrum matrix

$$\boldsymbol{S_w} = \begin{bmatrix} S_0 & \ldots & 0 \\ \vdots & \ddots & \vdots \\ 0 & \ldots & S_0 \end{bmatrix} \tag{5}$$

In passing, it is noted that the WPI technique, developed originally for Gaussian white noise excitation only [11], has been recently extended by Psaros et al. [17] to address general non-white, non-Gaussian and non-stationary cases decribed by Eqs. (3)-(4). In particular, differentiating Eq. (2) and substituting into Eq. (4) yields the 4th-order SDE

$$\Lambda_4 \boldsymbol{x}^{(4)} + \Lambda_3 \boldsymbol{x}^{(3)} + \Lambda_2 \ddot{\boldsymbol{x}} + \Lambda_1 \dot{\boldsymbol{x}} + \Lambda_0 \boldsymbol{x} + \boldsymbol{h}(\boldsymbol{x}, \dot{\boldsymbol{x}}, \ddot{\boldsymbol{x}}, \boldsymbol{x}^{(3)}) = \boldsymbol{w}(t) \tag{6}$$

where

$$\begin{cases} \Lambda_4 = \boldsymbol{P}\boldsymbol{D}^{-1}\boldsymbol{M} \\ \Lambda_3 = \boldsymbol{P}\boldsymbol{D}^{-1}\left[-2\dot{\boldsymbol{D}}\boldsymbol{D}^{-1}\boldsymbol{M} + \boldsymbol{C}\right] + \boldsymbol{Q}\boldsymbol{D}^{-1}\boldsymbol{M} \\ \Lambda_2 = \boldsymbol{P}\boldsymbol{D}^{-1}\left[\left(2\dot{\boldsymbol{D}}\boldsymbol{D}^{-1}\dot{\boldsymbol{D}}\boldsymbol{D}^{-1} - \ddot{\boldsymbol{D}}\boldsymbol{D}^{-1}\right)\boldsymbol{M} - 2\dot{\boldsymbol{D}}\boldsymbol{D}^{-1}\boldsymbol{C} + \boldsymbol{K}\right] \\ \qquad + \boldsymbol{Q}\boldsymbol{D}^{-1}\left(-\dot{\boldsymbol{D}}\boldsymbol{D}^{-1}\boldsymbol{M} + \boldsymbol{C}\right) + \boldsymbol{R}\boldsymbol{D}^{-1}\boldsymbol{M} \\ \Lambda_1 = \boldsymbol{P}\boldsymbol{D}^{-1}\left[\left(2\dot{\boldsymbol{D}}\boldsymbol{D}^{-1}\dot{\boldsymbol{D}}\boldsymbol{D}^{-1} - \ddot{\boldsymbol{D}}\boldsymbol{D}^{-1}\right)\boldsymbol{C} - 2\dot{\boldsymbol{D}}\boldsymbol{D}^{-1}\boldsymbol{K}\right] \\ \qquad + \boldsymbol{Q}\boldsymbol{D}^{-1}\left(-\dot{\boldsymbol{D}}\boldsymbol{D}^{-1}\boldsymbol{C} + \boldsymbol{K}\right) + \boldsymbol{R}\boldsymbol{D}^{-1}\boldsymbol{C} \\ \Lambda_0 = \boldsymbol{P}\boldsymbol{D}^{-1}\left(2\dot{\boldsymbol{D}}\boldsymbol{D}^{-1}\dot{\boldsymbol{D}}\boldsymbol{D}^{-1} - \ddot{\boldsymbol{D}}\boldsymbol{D}^{-1}\right)\boldsymbol{K} \\ \qquad - \boldsymbol{Q}\boldsymbol{D}^{-1}\dot{\boldsymbol{D}}\boldsymbol{D}^{-1}\boldsymbol{K} + \boldsymbol{R}\boldsymbol{D}^{-1}\boldsymbol{K} \end{cases} \tag{7}$$

and

$$\begin{aligned} \boldsymbol{h}(\boldsymbol{x}, \dot{\boldsymbol{x}}, \ddot{\boldsymbol{x}}, \boldsymbol{x}^{(3)}) &= \boldsymbol{P}\boldsymbol{D}^{-1}\ddot{\boldsymbol{g}}(\boldsymbol{x}, \dot{\boldsymbol{x}}) \\ &\quad + \left(-2\boldsymbol{P}\boldsymbol{D}^{-1}\dot{\boldsymbol{D}}\boldsymbol{D}^{-1} + \boldsymbol{Q}\boldsymbol{D}^{-1}\right)\dot{\boldsymbol{g}}(\boldsymbol{x}, \dot{\boldsymbol{x}}) \\ &\quad + \left[\boldsymbol{P}\boldsymbol{D}^{-1}\left(2\dot{\boldsymbol{D}}\boldsymbol{D}^{-1}\dot{\boldsymbol{D}}\boldsymbol{D}^{-1} - \ddot{\boldsymbol{D}}\boldsymbol{D}^{-1}\right)\right. \\ &\quad \left. - \boldsymbol{Q}\boldsymbol{D}^{-1}\dot{\boldsymbol{D}}\boldsymbol{D}^{-1} + \boldsymbol{R}\boldsymbol{D}^{-1}\right]\boldsymbol{g}(\boldsymbol{x}, \dot{\boldsymbol{x}}) + \boldsymbol{u}(\boldsymbol{x}, \dot{\boldsymbol{x}}, \ddot{\boldsymbol{x}}, \boldsymbol{x}^{(3)}) \end{aligned} \tag{8}$$

Notice that the differentiation of Eq. (2) yields time derivatives of order higher than 2 in Eqs. (6)–(8); i.e., $\boldsymbol{x}^{(3)}$ and $\boldsymbol{x}^{(4)}$ denoting the 3rd- and 4th-order derivatives of $\boldsymbol{x}(t)$, respectively.

Next, as shown in [17], the transition PDF $p\left(\boldsymbol{x}_f, \dot{\boldsymbol{x}}_f, \ddot{\boldsymbol{x}}_f, \boldsymbol{x}_f^{(3)}, t_f | \boldsymbol{x}_i, \dot{\boldsymbol{x}}_i, \ddot{\boldsymbol{x}}_i, \boldsymbol{x}_i^{(3)}, t_i\right)$ with $\left\{\boldsymbol{x}_i, \dot{\boldsymbol{x}}_i, \ddot{\boldsymbol{x}}_i, \boldsymbol{x}_i^{(3)}, t_i\right\}$ the initial state and $\left\{\boldsymbol{x}_f, \dot{\boldsymbol{x}}_f, \ddot{\boldsymbol{x}}_f, \boldsymbol{x}_f^{(3)}, t_f\right\}$ the final state can be written as

$$p\left(\boldsymbol{x}_f, \dot{\boldsymbol{x}}_f, \ddot{\boldsymbol{x}}_f, \boldsymbol{x}_f^{(3)}, t_f | \boldsymbol{x}_i, \dot{\boldsymbol{x}}_i, \ddot{\boldsymbol{x}}_i, \boldsymbol{x}_i^{(3)}, t_i\right) = \int_{\mathcal{C}\left\{\boldsymbol{x}_i, \dot{\boldsymbol{x}}_i, \ddot{\boldsymbol{x}}_i, \boldsymbol{x}_i^{(3)}, t_i; \boldsymbol{x}_f, \dot{\boldsymbol{x}}_f, \ddot{\boldsymbol{x}}_f, \boldsymbol{x}_f^{(3)}, t_f\right\}} \exp\left(-\int_{t_i}^{t_f} \mathcal{L}\left[\boldsymbol{x}, \dot{\boldsymbol{x}}, \ddot{\boldsymbol{x}}, \boldsymbol{x}^{(3)}, \boldsymbol{x}^{(4)}\right]\mathrm{d}t\right)\mathcal{D}[\boldsymbol{x}(t)] \tag{9}$$

where the Lagrangian $\mathcal{L}\left[\boldsymbol{x}, \dot{\boldsymbol{x}}, \ddot{\boldsymbol{x}}, \boldsymbol{x}^{(3)}, \boldsymbol{x}^{(4)}\right]$ is given by

$$\begin{aligned} \mathcal{L}\left[\boldsymbol{x}, \dot{\boldsymbol{x}}, \ddot{\boldsymbol{x}}, \boldsymbol{x}^{(3)}, \boldsymbol{x}^{(4)}\right] &= \frac{1}{2}\left[\Lambda_4 \boldsymbol{x}^{(4)} + \Lambda_3 \boldsymbol{x}^{(3)} + \Lambda_2 \ddot{\boldsymbol{x}} + \Lambda_1 \dot{\boldsymbol{x}} + \Lambda_0 \boldsymbol{x} + \boldsymbol{h}(\boldsymbol{x}, \dot{\boldsymbol{x}}, \ddot{\boldsymbol{x}}, \boldsymbol{x}^{(3)})\right]^T \\ &\quad \times \boldsymbol{B}^{-1}\left[\Lambda_4 \boldsymbol{x}^{(4)} + \Lambda_3 \boldsymbol{x}^{(3)} + \Lambda_2 \ddot{\boldsymbol{x}} + \Lambda_1 \dot{\boldsymbol{x}} + \Lambda_0 \boldsymbol{x} + \boldsymbol{h}(\boldsymbol{x}, \dot{\boldsymbol{x}}, \ddot{\boldsymbol{x}}, \boldsymbol{x}^{(3)})\right] \end{aligned} \tag{10}$$

where

$$\boldsymbol{B} = \begin{bmatrix} 2\pi S_0 & \ldots & 0 \\ \vdots & \ddots & \vdots \\ 0 & \ldots & 2\pi S_0 \end{bmatrix} \tag{11}$$

and $\mathcal{D}[\mathbf{x}(t)]$ is a functional measure [17]. In Eq. (9) $\mathcal{C}\left\{\mathbf{x}_i, \dot{\mathbf{x}}_i, \ddot{\mathbf{x}}_i, \mathbf{x}_i^{(3)}, t_i; \mathbf{x}_f, \dot{\mathbf{x}}_f, \ddot{\mathbf{x}}_f, \mathbf{x}_f^{(3)}, t_f\right\}$ denotes the set of all paths with initial state $\left\{\mathbf{x}_i, \dot{\mathbf{x}}_i, \ddot{\mathbf{x}}_i, \mathbf{x}_i^{(3)}\right\}$ at time t_i and final state $\left\{\mathbf{x}_f, \dot{\mathbf{x}}_f, \ddot{\mathbf{x}}_f, \mathbf{x}_f^{(3)}\right\}$ at time t_f.

The formal expression of the path integral in Eq. (9) is of little practical use as its analytical evaluation is highly challenging [14]. Therefore, an approximate approach is required. In this regard, the "most-probable path" approach (e.g., [10,14]) is employed, according to which the largest contribution to the transition PDF of Eq. (9) comes from the path $\mathbf{x}_c(t)$ that minimizes the integral in the exponential. In this regard, calculus of variations (e.g., [48]) dictates that the most probable path, $\mathbf{x}_c(t)$, satisfies the extremality condition

$$\delta \int_{t_i}^{t_f} \mathcal{L}\left[\mathbf{x}_c, \dot{\mathbf{x}}_c, \ddot{\mathbf{x}}_c, \mathbf{x}_c^{(3)}, \mathbf{x}_c^{(4)}\right] \mathrm{d}t = 0 \tag{12}$$

which yields the system of Euler-Lagrange (E-L) equations

$$\frac{\partial \mathcal{L}}{\partial x_{c,j}} - \frac{\partial}{\partial t}\frac{\partial \mathcal{L}}{\partial \dot{x}_{c,j}} + \frac{\partial^2}{\partial t^2}\frac{\partial \mathcal{L}}{\partial \ddot{x}_{c,j}} - \frac{\partial^3}{\partial t^3}\frac{\partial \mathcal{L}}{\partial x_{c,j}^{(3)}} + \frac{\partial^4}{\partial t^4}\frac{\partial \mathcal{L}}{\partial x_{c,j}^{(4)}} = 0, \quad \text{for } j = 1, \ldots, m \tag{13}$$

together with $8 \times m$ boundary conditions

$$\left.\begin{array}{l} x_{c,j}(t_i) = x_{j,i} \\ \dot{x}_{c,j}(t_i) = \dot{x}_{j,i} \\ \ddot{x}_{c,j}(t_i) = \ddot{x}_{j,i} \\ x_{c,j}^{(3)}(t_i) = x_{j,i}^{(3)} \\ x_{c,j}(t_f) = x_{j,f} \\ \dot{x}_{c,j}(t_f) = \dot{x}_{j,f} \\ \ddot{x}_{c,j}(t_f) = \ddot{x}_{j,f} \\ x_{c,j}^{(3)}(t_f) = x_{j,f}^{(3)} \end{array}\right\} \text{ for } j = 1, \ldots, m \tag{14}$$

Next, solving the boundary value problem (BVP) of Eqs. (13) and (14) yields the most probable path $\mathbf{x}_c(t)$ (m-dimensional), and the transition PDF from the initial state $\left\{\mathbf{x}_i, \dot{\mathbf{x}}_i, \ddot{\mathbf{x}}_i, \mathbf{x}_i^{(3)}, t_i\right\}$ to the final state $\left\{\mathbf{x}_f, \dot{\mathbf{x}}_f, \ddot{\mathbf{x}}_f, \mathbf{x}_f^{(3)}, t_f\right\}$ is determined as

$$p\left(\mathbf{x}_f, \dot{\mathbf{x}}_f, \ddot{\mathbf{x}}_f, \mathbf{x}_f^{(3)}, t_f | \mathbf{x}_i, \dot{\mathbf{x}}_i, \ddot{\mathbf{x}}_i, \mathbf{x}_i^{(3)}, t_i\right) = C \exp\left(-\int_{t_i}^{t_f} \mathcal{L}\left[\mathbf{x}_c, \dot{\mathbf{x}}_c, \ddot{\mathbf{x}}_c, \mathbf{x}_c^{(3)}, \mathbf{x}_c^{(4)}\right] \mathrm{d}t\right) \tag{15}$$

where the normalization constant C is evaluated based on the condition

$$\int_{-\infty}^{\infty} \cdots \int_{-\infty}^{\infty} p\left(\mathbf{x}_f, \dot{\mathbf{x}}_f, \ddot{\mathbf{x}}_f, \mathbf{x}_f^{(3)}, t_f | \mathbf{x}_i, \dot{\mathbf{x}}_i, \ddot{\mathbf{x}}_i, \mathbf{x}_i^{(3)}, t_i\right) \mathrm{d}\mathbf{x}_f \ldots \mathrm{d}\mathbf{x}_f^{(3)} = 1 \tag{16}$$

For the special case of time-modulated Gaussian white noise (i.e., $\boldsymbol{\xi}(t) = [\xi_1, \ldots, \xi_m]^T$ being a white noise stochastic vector process) Eq. (9) degenerates to

$$p(\mathbf{x}_f, \dot{\mathbf{x}}_f, t_f | \mathbf{x}_i, \dot{\mathbf{x}}_i, t_i) = \int_{\mathcal{C}\left\{\mathbf{x}_i, \dot{\mathbf{x}}_i, t_i; \mathbf{x}_f, \dot{\mathbf{x}}_f, t_f\right\}} \exp\left(-\int_{t_i}^{t_f} \mathcal{L}[\mathbf{x}, \dot{\mathbf{x}}, \ddot{\mathbf{x}}] \mathrm{d}t\right) \mathcal{D}[\mathbf{x}(t)] \tag{17}$$

and Eq. (15) becomes

$$p(\mathbf{x}_f, \dot{\mathbf{x}}_f, t_f | \mathbf{x}_i, \dot{\mathbf{x}}_i, t_i) = C \exp\left(-\int_{t_i}^{t_f} \mathcal{L}[\mathbf{x}_c, \dot{\mathbf{x}}_c, \ddot{\mathbf{x}}_c] \mathrm{d}t\right) \tag{18}$$

where

$$\mathcal{L}[\mathbf{x}, \dot{\mathbf{x}}, \ddot{\mathbf{x}}] = \tfrac{1}{2}(\boldsymbol{M}\ddot{\mathbf{x}} + \boldsymbol{C}\dot{\mathbf{x}} + \boldsymbol{K}\mathbf{x} + \boldsymbol{g}(\mathbf{x}, \dot{\mathbf{x}}))^T \widetilde{\boldsymbol{B}}^{-1} \\ \times (\boldsymbol{M}\ddot{\mathbf{x}} + \boldsymbol{C}\dot{\mathbf{x}} + \boldsymbol{K}\mathbf{x} + \boldsymbol{g}(\mathbf{x}, \dot{\mathbf{x}})) \tag{19}$$

$$\widetilde{\boldsymbol{B}} = \begin{bmatrix} 2\pi S_0 d_1^2(t) & \cdots & 0 \\ \vdots & \ddots & \vdots \\ 0 & \cdots & 2\pi S_0 d_m^2(t) \end{bmatrix} \tag{20}$$

and $\mathbf{x}_c(t)$ is the solution of the system of E-L equations

$$\frac{\partial \mathcal{L}}{\partial x_{c,j}} - \frac{\partial}{\partial t}\frac{\partial \mathcal{L}}{\partial \dot{x}_{c,j}} + \frac{\partial^2}{\partial t^2}\frac{\partial \mathcal{L}}{\partial \ddot{x}_{c,j}} = 0, \quad \text{for } j = 1, \ldots, m \tag{21}$$

together with $4 \times m$ boundary conditions

$$\left.\begin{array}{l} x_{c,j}(t_i) = x_{j,i} \\ \dot{x}_{c,j}(t_i) = \dot{x}_{j,i} \\ x_{c,j}(t_f) = x_{j,f} \\ \dot{x}_{c,j}(t_f) = \dot{x}_{j,f} \end{array}\right\} \quad \text{for } j = 1, \ldots, m \tag{22}$$

Finally, the normalization constant C can be determined by utilizing the condition

$$\int_{-\infty}^{\infty} \ldots \int_{-\infty}^{\infty} p(\mathbf{x}_f, \dot{\mathbf{x}}_f, t_f | \mathbf{x}_i, \dot{\mathbf{x}}_i, t_i) \mathrm{d}x_{1,f} \mathrm{d}\dot{x}_{1,f} \ldots \mathrm{d}x_{m,f} \mathrm{d}\dot{x}_{m,f} = 1 \tag{23}$$

It can be readily seen by comparing Eqs. (17) and (18) that in the approximation of Eq. (18) only a single trajectory, i.e., the most probable path $\mathbf{x}_c(t)$, is considered in evaluating the path integral of Eq. (17). Nevertheless, direct comparisons of Eq. (18) with pertinent MCS data related to various engineering dynamical systems have demonstrated a high degree of accuracy [15,17].

Further, considering fixed initial conditions $(\mathbf{x}_i, \dot{\mathbf{x}}_i)$ typically (i.e., system initially at rest), the solution of a functional minimization problem (i.e., Eqs. (21)-(22)) for determining a single point of the joint response PDF is required. Utilizing a data analysis perspective and terminology, this can be construed as obtaining joint response PDF measurements at pre-specified sampling locations.

2.2. Numerical implementation aspects

In general, a numerical solution scheme needs to be implemented for the BVP of Eqs. (21) and (22) (or of Eqs. (13) and (14) for non-white and non-Gaussian excitation). Without loss of generality and considering fixed initial conditions, the only variables describing the PDF $p(\mathbf{x}_f, \dot{\mathbf{x}}_f, t_f | \mathbf{x}_i, \dot{\mathbf{x}}_i, t_i)$ at a time instant t_f are $\mathbf{x}_f$ and $\dot{\mathbf{x}}_f$. In this regard, dropping the subscript f for simplicity and adopting a brute-force numerical solution approach, for each time instant t an effective domain of values is considered for the joint response PDF $p(\mathbf{x}, \dot{\mathbf{x}}, t)$. Next, discretizing the effective domain using N_s points in each dimension, the joint response PDF values are obtained corresponding to the points of the mesh. More specifically, for an m-DOF system corresponding to $2m$ stochastic dimensions (m displacements and m velocities) the number of measurements required is N_s^{2m}. These $2m$ stochastic dimensions will be referred to hereinafter as spatial dimensions. Clearly, the computational cost related to a brute-force solution scheme implementation becomes prohibitive eventually, especially for high-dimensional systems.

To address the above computational challenge, Kougioumtzoglou et al. [19] employed a polynomial expansion for the logarithm of the joint response PDF; thus, the number of required PDF measurements becomes equal to the number of the expansion coefficients. The rationale for selecting a polynomial expansion relates to the fact that in cases of linear systems (i.e., $\mathbf{g}(\mathbf{x}, \dot{\mathbf{x}}) = 0$) the joint response PDF is Gaussian, or, in other words, the function $\log(p(\mathbf{x}, \dot{\mathbf{x}}, t))$ can be expressed exactly as a second-order polynomial. In the general case, where $\mathbf{g}(\mathbf{x}, \dot{\mathbf{x}}) \neq 0$, $p(\mathbf{x}, \dot{\mathbf{x}}, t)$ can be construed as a "perturbation" (not necessarily small) from the Gaussian PDF, and, thus, more monomials are required to enhance the approximation accuracy. The resulting polynomial is, consequently, of higher order. Further, it was shown that the computational cost follows approximately a power-law function of the form $\sim (2m)^\lambda / \lambda!$ (where λ is the degree of the polynomial), which can be orders of magnitude smaller than N_s^{2m}. Moreover, it has been recently shown by Psaros et al. [20] that a compressive sampling treatment in conjunction with an appropriate optimization algorithm can further reduce drastically the required number of PDF measurements (i.e., number of deterministic BVPs to be solved numerically).

Nevertheless, all the above enhancements in terms of computational efficiency of the WPI technique relate to determining the joint response PDF at a specific fixed final time instant t. In other words, in cases where the determination of the complete time-dependent non-stationary response PDF is of interest, the procedure should be applied for each and every time instant. Indicatively, the joint response PDF of a 10-DOF nonlinear dynamical system at a given time instant has been obtained with only $n_s = 3,200$ measurements as shown in [20], whereas a brute-force PDF domain discretization scheme would require 30^{20} measurements (for $N_s = 30$). However, even with the efficient implementation of [20], a brute-force discretization of the time domain (temporal dimension) into $N_t = 1,000$ points, for instance, would still require $N_t n_s = 3.2 \times 10^6$ PDF measurements. In this paper, motivated by the aforementioned challenge, the computational efficiency of the WPI is further increased by resorting to expansions based on Kronecker products of basis matrices (Section 3.1) and on positive definite functions (Section 3.2). In this regard, the WPI technique is enhanced herein and becomes capable of determining directly the global time-dependent non-stationary joint response PDF in a computationally efficient manner.

3. Non-stationary joint response PDF approximation

As discussed in Section 2.2, the computational cost associated with determining the global non-stationary joint response PDF by applying a brute-force discretization of the time domain remains significant, even when using the efficient implementations of [19,20]. To address this challenge, the approximation schemes developed in this section consider the response PDF as a function of time explicitly. In this regard, generalizing the formulations of [19,20], $p(\mathbf{x}, \dot{\mathbf{x}}, t)$ is written as

$$p(\mathbf{x}, \dot{\mathbf{x}}, t) \approx \exp\left(\mu(\mathbf{x}, \dot{\mathbf{x}}, t)\right) \tag{24}$$

or, alternatively, as

$$p(\mathbf{x}, \dot{\mathbf{x}}, t) \approx v(\mathbf{x}, \dot{\mathbf{x}}, t) \tag{25}$$

where $\mu(\mathbf{x}, \dot{\mathbf{x}}, t)$ and $v(\mathbf{x}, \dot{\mathbf{x}}, t)$ are approximating functions. Therefore, depending on whether Eq. (24) or Eq. (25) is used, a measurement of the response PDF at a specific location $(\mathbf{x}, \dot{\mathbf{x}}, t)$ via the WPI technique refers to either the exponent or the exponential function of Eq. (18), respectively.

First, in Section 3.1, a separable basis is constructed for approximating the non-stationary PDF by combining the bases/structures selected for each dimension [49]. Such a basis proves, in general, capable of handling the anisotropic features of multivariate functions and appears a natural choice for approximating the response PDF. Next, an alternative approach is followed in Section 3.2, where the approximation takes the form of a scattered data fitting problem [50]. The non-stationary PDF is sampled at various locations in the spatio-temporal domain and a fit to the dataset based on positive definite functions (which can be construed as a generalization of the widely used RBFs [50]) is sought for. Also, it is noted that positive definite functions have been deliberately selected over RBFs for better coping with the potentially anisotropic features of the non-stationary PDF [50].

3.1. Kronecker product approach

3.1.1. Kronecker product bases
Various multivariate bases have been developed based on Kronecker products [51]. Remarkably, the applications of Kronecker structure range from image/video processing [52] and distributed sensing [49] to pre-conditioning for linear system solution [53] and matrix approximation [54].

Specifically, the Kronecker product $\mathbf{H} \otimes \mathbf{J}$ of two matrices $\mathbf{H} \in \mathbb{R}^{H_1 \times H_2}$ and $\mathbf{J} \in \mathbb{R}^{J_1 \times J_2}$ is a matrix of size $H_1 J_1 \times H_2 J_2$ defined by (e.g., [51])

$$\mathbf{H} \otimes \mathbf{J} = \begin{bmatrix} h_{11}\mathbf{J} & \dots & h_{1H_2}\mathbf{J} \\ \vdots & \ddots & \vdots \\ h_{H_1 1}\mathbf{J} & \dots & h_{H_1 H_2}\mathbf{J} \end{bmatrix} \tag{26}$$

Further, given the basis matrices $\mathbf{D}_1 \in \mathbb{R}^{n_1 \times n_1}$ and $\mathbf{D}_2 \in \mathbb{R}^{n_2 \times n_2}$, consider a transform applied to a data matrix $\mathbf{Y} \in \mathbb{R}^{n_1 \times n_2}$ by using the separable basis constructed by their Kronecker product. Vectorizing matrix $\mathbf{Y}$, i.e., concatenating its columns vertically, so that $\mathbf{y} = vec(\mathbf{Y}) \in \mathbb{R}^{n_1 n_2}$, the data vector can be written as (e.g., [51])

$$\mathbf{y} = (\mathbf{D}_2 \otimes \mathbf{D}_1)\mathbf{c} \tag{27}$$

where $\mathbf{c}$ denotes the coefficient matrix in vectorized form. Generalizing, consider p dimensions in total and $n_1 n_2 \dots n_p$ measurements taken from a multivariate function $y(\mathbf{q})$, where $\mathbf{q} \in \mathbb{R}^p$. The measurement tensor $\mathbf{Y} \in \mathbb{R}^{n_1 \times n_2 \times \dots \times n_p}$ admits a Kronecker expansion of the form of Eq. (27) expressed as

$$\mathbf{y} = \left(\mathbf{D}_p \otimes \dots \otimes \mathbf{D}_2 \otimes \mathbf{D}_1\right)\mathbf{c} \tag{28}$$

where $\mathbf{y}, \mathbf{c} \in \mathbb{R}^{n_1 n_2 \dots n_p}$. Therefore, after collecting $n = n_1 n_2 \dots n_p$ measurements from the p-dimensional space and selecting a basis in each dimension $(\mathbf{D}_1, \dots, \mathbf{D}_p)$ the coefficients of the Kronecker expansion can be obtained by solving the linear system of Eq. (28). It is noted that the columns of the basis matrices $\mathbf{D}_1, \dots, \mathbf{D}_p$ in Eq. (28) are the basis functions selected for each dimension discretized into $n_1, \dots, n_p$ points, respectively.

3.1.2. Multi-dimensional basis construction for approximating the non-stationary joint response PDF
Following the procedure outlined in Section 3.1.1 it is rather straightforward to construct a multi-dimensional basis for approximating the non-stationary response PDF by employing Eqs. (25) and (28). Specifically, the response PDF is a function of $(\mathbf{x}, \dot{\mathbf{x}}, t)$, which is of size $2m + 1$; that is, $2m$ spatial dimensions and 1 temporal dimension. In this regard, various (potentially different) bases can be chosen for the approximation in each dimension in conjunction with the numbers $n_k, k \in \{1, \dots, 2m + 1\}$. Next, the expansion coefficients vector $\mathbf{c}$ is determined by solving the linear system of Eq. (28), where $\mathbf{y}$ is the vector containing $n_1 \dots n_{2m+1}$ measurements of $p(\mathbf{x}, \dot{\mathbf{x}}, t)$ determined via WPI and employing a uniform mesh. In the following, and without loss of generality, two distinct approaches are pursued in choosing the bases to be utilized in Eq. (28).

First, the same one-dimensional wavelet basis is used for each and every dimension. In particular, an arbitrary function $f(t)$ can be expressed as

$$f(t) = \sum_{l=-\infty}^{\infty} \sum_{r=-\infty}^{\infty} c_{lr} \psi_{lr}(t) \tag{29}$$

where c are the expansion coefficients to be determined, r and l denote the different scales and translation levels, respectively, and $\psi_{lr}(t) = \frac{1}{2^l} \psi \left(\frac{t}{2^l} - r \right)$, with $\psi(t)$ the wavelet family to be chosen. Alternatively, Eq. (29) can be expressed via the associated scaling function $\phi(t)$ as

$$f_n(t) = \sum_{r=0}^{n-1} c_r \phi_{Lr}(t) \tag{30}$$

where $f_n(t)$ denotes the n-term approximation of the function $f(t)$ with only $n = 2^{-L}$ scaling functions, given as $\phi_{Lr}(t) = \frac{1}{2^L} \phi \left(\frac{t}{2^L} - r \right)$, and L denotes the selected scale, or equivalently the approximation level. A detailed presentation of wavelet theory can be found in several books, such as [55]. Obviously, the efficacy of the chosen wavelet family is application-dependent. Thus, various both discrete and continuous wavelets have been developed over the past decades [55], as well as generalizations with additional parameters such as harmonic wavelets (e.g., [56–58]) and chirplets (e.g., [59]); see also the review paper by Spanos and Failla [60] for diverse wavelet applications in engineering dynamics. In the ensuing analysis, the Meyer wavelet (e.g., [55]) is used in the related expansions.

Second, an alternative approach is pursued, which exploits the flexibility of the herein proposed framework to use different bases. In this regard, and considering Eq. (24), a multivariate polynomial can be employed for the spatial dimensions, as in [19], and a wavelet basis for the temporal dimension. Therefore, the linear system of Eq. (27) becomes

$$\boldsymbol{y} = (\boldsymbol{D}_w \otimes \boldsymbol{P}) \boldsymbol{c} \tag{31}$$

where $\boldsymbol{y}$ contains the measurements of $\log (p(\boldsymbol{x}, \dot{\boldsymbol{x}}, t))$ determined via the WPI, $\boldsymbol{D}_w$ denotes the one-dimensional wavelet basis, $\boldsymbol{P}$ the monomial basis (e.g., [61]) and $\boldsymbol{c}$ the coefficient vector. Specifically, $\boldsymbol{P}$ is an $n_s \times n_s$ matrix, where $n_s = \binom{\lambda+2m}{2m}$ for a polynomial of degree λ, and $\boldsymbol{D}_w$ is an $n_t \times n_t$ matrix. Therefore, $n = n_s n_t$ measurements of the joint response PDF via the WPI technique are required.

Overall, it is readily seen that utilizing a Kronecker product formulation is a conceptually simple approach for higher-dimensional approximations by combining several lower-dimensional approximations in a straightforward manner. This yields enhanced flexibility in the implementation of the approach as various, potentially different, bases can be used, which have already proven to be well-suited for the respective lower-dimensional problems. For instance, the monomial basis has exhibited significant accuracy in approximating the spatial dimensions of a class of problems in [19] and in [20]. Thus, under the Kronecker product formulation, it can be directly used in conjunction with an additional basis related to the temporal dimension. Nevertheless, the lower-dimensional bases and the respective number of measurements need to be selected a priori, while as noted in [20], the monomial basis is prone to ill-conditioning, and, hence, the points of the mesh should be selected based on certain optimality criteria for enhanced robustness and accuracy of the approximation (see for instance [62]). If, alternatively, only one-dimensional wavelet bases are used for constructing the multi-dimensional basis via Eq. (28), the associated computational cost increases exponentially with increasing number of dimensions and becomes eventually prohibitive for relatively high-dimensional problems. .

To address the above points, a mesh-free approximation scheme is developed in Section 3.2 by utilizing positive definite functions. The advantages of such an approach pertain mainly to the fact that the basis functions depend on the measurement locations, and thus, are not selected a priori. Therefore, as explained in detail in Section 3.2, the resulting interpolation matrix is well-conditioned yielding a robust and accurate approximation. Overall, positive definite functions appear more general and suitable for higher-dimensional systems, whereas Kronecker product bases perform better for lower-dimensional systems, especially when there is some available information regarding the response PDF.

3.2. Positive definite functions approach

3.2.1. Positive definite functions aspects

In this section, the multivariate (p-dimensional) approximation problem is formulated as a scattered data fitting problem, which is a fundamental problem in approximation theory and is summarized in the following [50]: Given a set of measurements $(\boldsymbol{q}_i, y_i)$ from a function $y(\boldsymbol{q}_i)$, where $i \in \{1, \dots, n\}, \boldsymbol{q}_i \in \mathbb{R}^p$ and $y_i \in \mathbb{R}$, determine a function $\mu(\boldsymbol{q})$ such that

$$\mu(\boldsymbol{q}_i) = y_i \tag{32}$$

$\forall\, i \in \{1, \dots, n\}$. Even though in the univariate case (i.e., $p = 1$) this meshfree problem has a unique solution using n distinct measurements and a polynomial of order $n - 1$, the multivariate case is more complex leading to ill-conditioned interpolation matrices [63]. According to the Mairhuber-Curtis theorem (e.g., [64]), for the problem to be well-posed, i.e., for a solution to exist and be unique, the basis functions cannot be fixed a priori.

The above challenge has led mathematicians to introduce data-dependent bases, which are bases created following the selection of the sampling locations. In this direction, positive definite functions (or kernels more generally) have been commonly used in approximation theory [50,65]. Following [63], a complex-valued continuous function $\Phi : \mathbb{R}^p \to \mathbb{C}$ is called positive definite on $\mathbb{R}^p$ if

$$\sum_{i=1}^{n}\sum_{j=1}^{n} c_i \bar{c}_j \Phi(\boldsymbol{q}_i - \boldsymbol{q}_j) \geqslant 0 \tag{33}$$

for any n pairwise different points $\boldsymbol{q}_1, \ldots, \boldsymbol{q}_n \in \mathbb{R}^p$ and $\boldsymbol{c} = [c_1, \ldots, c_n]^T \in \mathbb{C}^n$. Among the most widely used positive definite functions is the Gaussian function, i.e., $\Phi(\boldsymbol{q}) = e^{-\epsilon^2 \|\boldsymbol{q}\|_2^2}$, with $\boldsymbol{q} \in \mathbb{R}^p$ and a shape parameter $\epsilon > 0$. The widespread utilization of positive definite functions in the approximation field can be attributed, at least partly, to their connection with the scattered data fitting problem of Eq. (32), and to the existence of well-behaved (i.e., non-singular) interpolation matrices (e.g., [66]). Further, there are constantly new classes of positive definite functions being introduced in conjunction with related theoretical work on error bounds [63]. Finally, it is worth noting that the numerical implementation of positive definite functions is amenable to high-performance computing [67], while their applications range from meshfree interpolation and solution of partial differential equations (PDEs) [68] to simulation of stochastic processes [69] and machine learning [70].

3.2.2. Multi-dimensional basis construction for approximating the non-stationary joint response PDF

As mentioned in Section 3.2.1, given the measurements $(\boldsymbol{q}_i, y_i)$ the objective is to determine an interpolating function $\mu(\boldsymbol{q})$, expressed as

$$\mu(\boldsymbol{q}) = \sum_{i=1}^{n} c_i \Phi_i(\boldsymbol{q}) \tag{34}$$

where the basis functions Φ_i, for $i \in \{1, \ldots, n\}$, are positive definite and $\boldsymbol{c} = [c_1, \ldots, c_n]^T \in \mathbb{R}^n$ denotes the expansion coefficient vector. Clearly, the choice of the specific basis functions is problem-dependent, with RBFs being among the most popular choices [71]. RBFs are rotationally and translationally invariant and are commonly used in engineering problems. For RBF interpolation the basis functions are expressed as a function of $\|\boldsymbol{q} - \boldsymbol{q}_i\|$, where $\boldsymbol{q}_i$, for $i \in \{1, \ldots, n\}$, corresponds to the sampling locations.

Alternative choices include, but are not limited to, multiscale kernels [72], which are defined as linear combinations of shifted and scaled versions of a single function and exhibit properties similar to wavelets, and translationally invariant functions [50]. The latter are constructed by relaxing the rotational invariance property of RBFs and have been found to provide further flexibility in the interpolation and to improve the condition number of the interpolation matrix [50]. A typical example that is also adopted in the ensuing analysis is the anisotropic multivariate Gaussian function

$$\Phi_i(\boldsymbol{q}) = \exp\left(-\sum_{k=1}^{p} \epsilon_k^2 (q_k - q_{ik})^2\right) \tag{35}$$

where ϵ_k, for $k \in \{1, \ldots, p\}$, denotes the shape parameter for the k-th dimension, while q_k and q_{ik} denote the k-th component of $\boldsymbol{q}$ and $\boldsymbol{q}_i$, respectively. The basis then becomes a collection of functions of the form of Eq. (35), i.e.,

$$\{\Phi_1(\boldsymbol{q}), \ldots, \Phi_n(\boldsymbol{q})\} \tag{36}$$

Next, considering $\boldsymbol{q} = (\boldsymbol{x}, \dot{\boldsymbol{x}}, t)$ yields $p = 2m + 1$ dimensions, while the same shape parameter value ϵ_s is used for all the spatial dimensions and the value ϵ_t for the temporal dimension. In this regard, by employing anisotropic Gaussian functions, Eq. (24) becomes

$$p(\boldsymbol{x}, \dot{\boldsymbol{x}}, t) \approx \exp\left[\sum_{i=1}^{n} c_i \exp\left(-\sum_{k=1}^{m} \epsilon_s^2 (x_k - x_{ik})^2 - \sum_{k=1}^{m} \epsilon_s^2 (\dot{x}_k - \dot{x}_{ik})^2 - \epsilon_t^2 (t - t_i)^2\right)\right] \tag{37}$$

Note that the n sampling locations need to be well-distributed in the $(2m + 1)$-space. To this aim, the Halton sequence is used [73], which is also frequently employed in quasi-Monte Carlo methods for multi-dimensional integration; see also the papers by Bratley et al. [74] and by De Marchi et al. [75] for some alternative sampling strategies. Further, it is desirable in many cases to have an interpolant that exactly reconstructs a polynomial of a given order; see, for instance, the "patch test" in finite elements (e.g., [76]). To this aim, the basis of Eq. (36) can be augmented by including monomials to a given order; that is

$$\{\Phi_1(\boldsymbol{q}), \ldots, \Phi_n(\boldsymbol{q}), 1, q_1, q_2, \ldots, q_1^2, 2q_1 q_2, \ldots\} \tag{38}$$

Therefore, the size of the basis of Eq. (38) becomes $n + n_p$, where n is the number of measurements, and $n_p = \binom{\lambda + 2m + 1}{2m + 1}$ is the number of monomials $P_u(\boldsymbol{q}), u \in \{1, \ldots, n_p\}$, for a polynomial of degree λ. In the following, a 4th-degree polynomial is considered in the augmented basis of Eq. (38), in accordance with the rationale presented in [20]. Concisely, for problems of the form of Eq. (2), the joint response PDF is Gaussian for $\boldsymbol{g}(\boldsymbol{x}, \dot{\boldsymbol{x}}) = \boldsymbol{0}$; thus, it is represented exactly by a 2nd-degree polyno-

mial. The nonlinear system joint response PDF can be construed as a perturbation (not necessarily small) from the Gaussian, and it can be approximated by higher-order polynomials. In several examples, including rather challenging cases of bimodal response PDFs [20], it has been demonstrated that the choice of a 4th-degree polynomial reflects a reasonable compromise between accuracy and efficiency. In this regard, enforcing the n interpolation conditions of Eq. (34) and adding n_p conditions of the form

$$\sum_{i=1}^{n} c_i P_u(\boldsymbol{q}_i) = 0, \quad \text{for } u \in \{1, \ldots, n_p\} \tag{39}$$

leads to the augmented linear system of equations [63]

$$\begin{bmatrix} \boldsymbol{\Phi} & \boldsymbol{P} \\ \boldsymbol{P}^T & \boldsymbol{0} \end{bmatrix} \begin{bmatrix} \boldsymbol{c} \\ \boldsymbol{c}_p \end{bmatrix} = \begin{bmatrix} \boldsymbol{y} \\ \boldsymbol{0} \end{bmatrix} \tag{40}$$

where $\boldsymbol{\Phi} = [\Phi_1(\boldsymbol{q}_i), \ldots, \Phi_n(\boldsymbol{q}_i)]_{n \times n}, \boldsymbol{P} = [P_u(\boldsymbol{q}_i)]_{n \times n_p}, \boldsymbol{c}$ denotes the expansion coefficients vector, $\boldsymbol{c}_p$ the polynomial coefficients vector, and $\boldsymbol{y}$ the measurement vector. It is noted that the conditions of Eq. (39) are arbitrary and have been added for obtaining a non-singular interpolation matrix [63]. Once the system of Eq. (40) is solved, the coefficient vector $[\boldsymbol{c}; \boldsymbol{c}_p]$ is determined; see also [77] for more details on the conditions to be satisfied for the well-posedness of Eq. (40). Note that although the augmented coefficient vector of Eq. (40) is of length $n + n_p > n$, the number of measurements required for the approximation remains the same and equal to n. Further, Eq. (37) is modified to account for the augmented basis, and the non-stationary joint response PDF can be approximated as

$$p(\boldsymbol{x}, \dot{\boldsymbol{x}}, t) \approx \exp\left(\sum_{i=1}^{n} c_i \Phi_i(\boldsymbol{x}, \dot{\boldsymbol{x}}, t) + \sum_{u=1}^{n_p} c_{pu} P_u(\boldsymbol{x}, \dot{\boldsymbol{x}}, t)\right) \tag{41}$$

3.2.3. Selection of shape parameters

Positive definite functions have been criticized for producing ill-conditioned interpolation matrices $\boldsymbol{\Phi}$, and thus, causing numerical instability issues [78]. Note, however, that a careful examination of the matter [63] reveals that there is a trade-off between accuracy and stability. Theoretical bounds pertaining to several positive definite functions indicate that by decreasing the values of the shape parameters ϵ_k in Eq. (35), or the separation distance between the sampling locations (i.e., by increasing n), the accuracy of the interpolation is improved. Nevertheless, this theoretically attainable accuracy is hard to be reached in practice. This is due to numerical stability issues related to the rapid increase of the interpolation matrix condition number. This trade-off has led researchers to seek for "optimal" shape parameters, which provide high accuracy without compromising numerical stability [79].

The approach adopted in the ensuing analysis was developed in [80] and is based on leave-one-out cross validation. Specifically, for fixed shape parameters ϵ_s and ϵ_t, fitting an interpolant of the form of Eqs. (34) and (40) to $n - 1$ measurements n times (one is left out each time) yields an interpolation error E_i, for $i \in \{1, \ldots, n\}$, by comparing the interpolant with the measurement left out. The error, E, associated with the pair (ϵ_s, ϵ_t) is then selected to be the maximum of all the errors E_i. Therefore, the error associated with the pair (ϵ_s, ϵ_t) becomes the cost function in an optimization algorithm that searches for the pair (ϵ_s, ϵ_t) with the minimum error E. Finally, as stated in Section 3.2.2, introducing the anisotropic Gaussian function of Eq. (35) also improves the condition number of the interpolation matrix as a "side-effect". Of course, alternative approaches such as pre-conditioning [63], or exploration of other bases [81], can always be used for addressing cases of ill-conditioned matrices.

3.3. Mechanization of the technique

The mechanization of the Kronecker product approach of Section 3.1 involves the following steps:

(a) Select p lower dimensional bases $\boldsymbol{D}_1, \ldots, \boldsymbol{D}_p$.
(b) Create the interpolation matrix $\boldsymbol{D} = \boldsymbol{D}_p \otimes \ldots \otimes \boldsymbol{D}_2 \otimes \boldsymbol{D}_1$.
(c) Obtain $n = n_1 n_2 \ldots n_p$ measurements of the PDF via the WPI by utilizing Eq. (18).
(d) Determine the coefficient vector $\boldsymbol{c}$ by solving the linear system of Eq. (28).
(e) The complete non-stationary joint response PDF is evaluated by employing the Kronecker product basis and the coefficient vector via Eqs. (25) and (28).

Further, the mechanization of the positive definite functions approach of Section 3.2 involves the following steps:

(a) Select the n basis functions of Eq. (38), in conjunction with Eq. (35).
(b) Obtain n measurements of the PDF via the WPI by utilizing Eq. (18) and by employing the Halton sequence for selecting the locations of the measurements [73].
(c) Determine the coefficient vector $\boldsymbol{c}$ by solving the linear system of Eq. (40).
(d) The complete non-stationary joint response PDF is approximated via Eq. (41).

4. Numerical examples

To assess the performance and demonstrate the efficacy of the developed approximation schemes, three examples with distinct features are considered. In Section 4.1, two single-degree-of-freedom (SDOF) Duffing nonlinear oscillators subject to Gaussian white noise are considered: one with a standard hardening restoring force (Section 4.1.1), and another exhibiting a bimodal response PDF (Section 4.1.2). In Section 4.1.1 the Kronecker product approach with a 4th-degree polynomial for the spatial dimensions and a one-dimensional wavelet basis for the temporal dimension is used, whereas in Section 4.1.2 a basis constructed via a Kronecker product of three one-dimensional wavelet bases is employed. Next, in Section 4.2 a 2-DOF non-linear oscillator subject to non-stationary time-modulated Gaussian white noise is considered, and the positive definite functions approach of Section 3.2 is employed. Finally, the positive definite functions approach is also employed in Section 4.3, where a statically determinate Euler-Bernoulli beam is considered with Young's modulus modeled as a non-Gaussian, non-white and non-homogeneous stochastic field.

4.1. SDOF Duffing nonlinear oscillator

4.1.1. SDOF Duffing oscillator with a hardening restoring force

Consider an SDOF Duffing oscillator, whose equation of motion is given by Eq. (2) with parameter values ($\boldsymbol{M} = 1; \boldsymbol{C} = 0.1; \boldsymbol{K} = 1; \boldsymbol{g} = x^3$). The stochastic excitation is given by Eq. (3) with $\boldsymbol{D}(t) = 1$ and $\xi(t)$ is a white noise process. Therefore, $f(t)$ is a Gaussian white noise process, whose power spectrum is given by Eq. (5) with $S_0 = 0.0637$. Assuming quiescent initial conditions, its transition PDF, written as $p(x, \dot{x}, t)$, is a function of the two spatial dimensions, i.e., x and $\dot{x}$, and of the temporal dimension t. In implementing the approximate WPI technique developed herein, the monomial basis is used for the two spatial dimensions, while the wavelet basis is used for the temporal dimension as discussed in Section 3.1.2. In particular, utilizing a 4th-degree polynomial, the joint response PDF is sampled at $n = n_s n_t = 15 \times 32 = 480$ locations in the spatio-temporal domain and the expansion coefficient vector $\boldsymbol{c}$ is determined by solving Eq. (31). Finally, $p(x, \dot{x}, t)$ is approximated by utilizing the constructed basis and the coefficient vector via Eq. (28). The non-stationary marginal PDFs of $x(t)$ and $\dot{x}(t)$ are shown in Fig. 1, where it is seen that the oscillator response PDF does not experience any significant changes after about $t = 6$s; that is, the system has reached stationarity effectively. Moreover, the marginal PDFs of $x(t)$ and $\dot{x}(t)$ for two arbitrary time instants are shown in Fig. 2. Although the accuracy of the technique depends, in general, on the choice of the polynomial degree and the number of points in the temporal dimension, it is shown in this example that a 4th-degree polynomial and $n_t = 32$ points are adequate in determining the non-stationary PDF of this Duffing oscillator with high accuracy as compared to pertinent MCS data (50,000 realizations).

To provide a rough comparison and highlight the gain of the proposed technique in terms of computational efficiency, it is worth noting that a brute-force numerical implementation of the WPI technique as described in Section 2.2 would require a number of PDF measurements of the order of $\sim 10^6$ (assuming that the temporal dimension is, indicatively, discretized into 1,000 points). Further, the approximation based on polynomials and wavelets employed in this example also requires a smaller number of measurements as compared to the efficient implementation of [19]. Specifically, by utilizing the approximate technique developed in [19] the response PDF needs to be separately determined at every time instant, which (for an indicative discretization of the time domain into 1,000 points) yields approximately 35,000 required PDF measurements via the WPI technique.

4.1.2. SDOF Duffing oscillator with a bimodal response PDF

Although Example 4.1.1 has shown that utilizing a Kronecker product of a polynomial and a wavelet bases can be adequate for a certain class of problems, the resulting interpolation matrix may often be ill-conditioned. Such is the case of the SDOF oscillator, whose equation of motion is given by Eq. (2) with parameter values ($\boldsymbol{M} = 1; \boldsymbol{C} = 1; \boldsymbol{K} = -0.3; \boldsymbol{g} = x^3$) and external excitation as in Example 4.1.1. In fact, attempting to use the same basis as in 4.1.1 has led to ill-conditioning. To bypass this limitation, a multi-dimensional wavelet basis is instead utilized for this case, as discussed in Section 3.1.2. In this regard, a mesh is employed for discretizing the three-dimensional spatio-temporal domain characterizing the transition PDF. Specifically, following the procedure delineated in Section 3.1.2 the two spatial dimensions are discretized into $n_1 = n_2 = 16$ points and the temporal dimension into $n_t = 32$ points; thus, yielding $n = 8,192$ required measurements via the WPI technique. To put it into perspective, note that a brute-force implementation of the technique would require a number of PDF measurements of the order of $\sim 10^6$, while applying the efficient implementation of [19] for each and every time instant would yield approximately 35,000 required measurements (assuming that the temporal dimension is, indicatively, discretized into 1,000 points). Following the determination of the expansion coefficient vector $\boldsymbol{c}$ by solving Eq. (28), where all basis matrices correspond to the wavelet basis in each dimension, $p(x, \dot{x}, t)$ is approximated based on Eq. (25). In this regard, $p(x, \dot{x}, t)$ can be approximated at any location by utilizing the constructed basis and the coefficient vector. In Fig. 3 the joint response PDF $p(x, \dot{x}, t)$ is shown at three arbitrary time instants $t = 1, 2$ and 6s. Comparisons with corresponding MCS based results demonstrate the relatively high accuracy of the technique for addressing dynamical systems even with relatively complex PDF shapes, such as the bimodal. Finally, in Figs. 4 and 5 the marginal PDFs of $x(t)$ and $\dot{x}(t)$ are shown for various time instants, as obtained by utilizing the herein developed technique. Pertinent MCS based
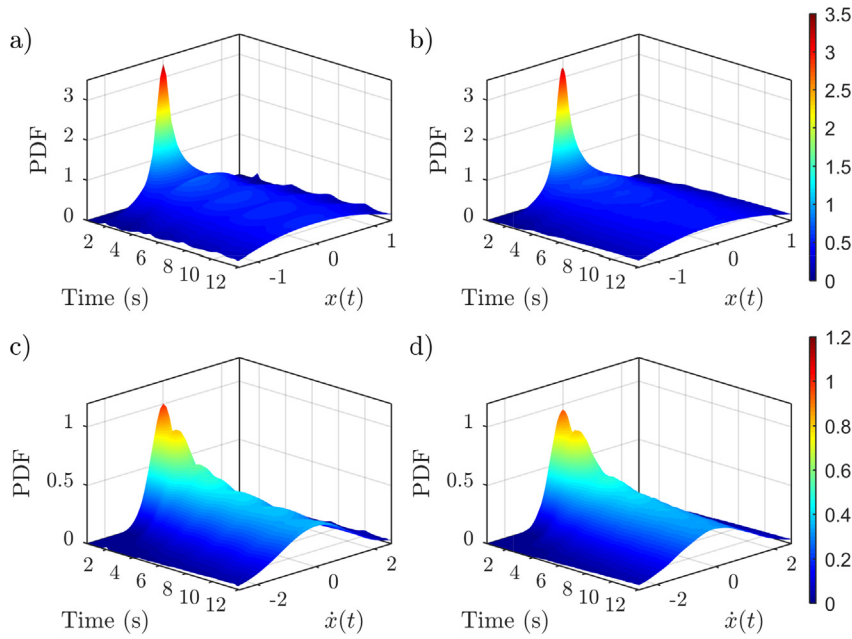
Fig. 1. Non-stationary marginal PDF of $x(t)$ and $\dot{x}(t)$ for an SDOF hardening Duffing oscillator under Gaussian white noise excitation, as obtained via the WPI technique (a and c); comparisons with MCS data – 50,000 realizations (b and d).
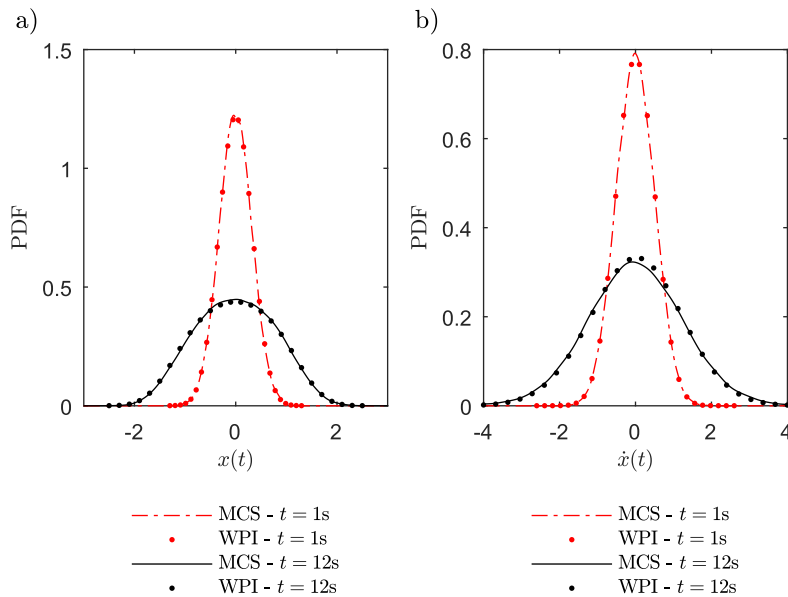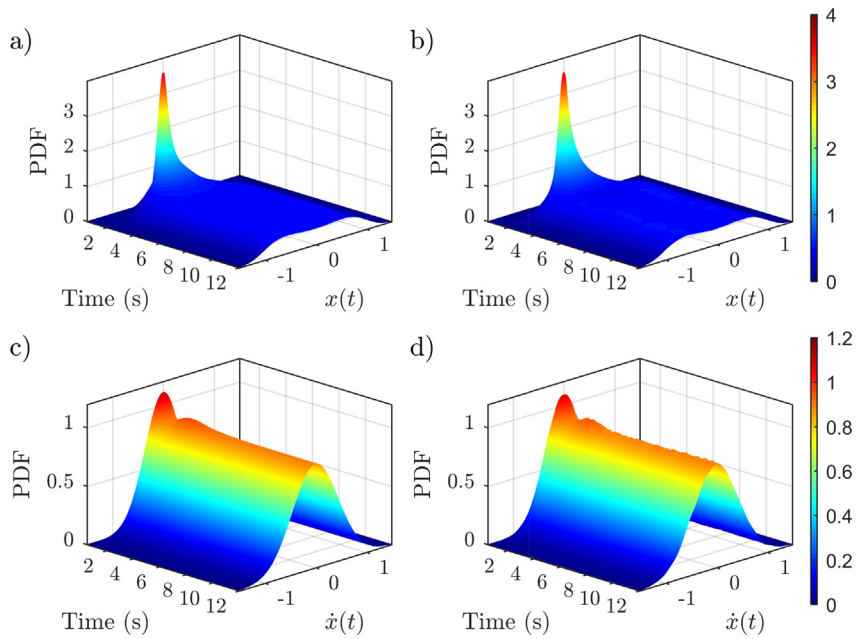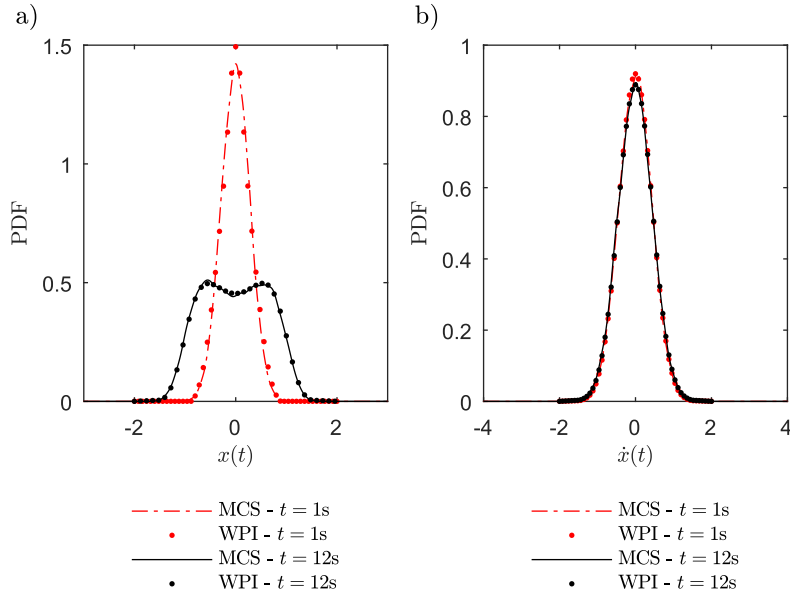

Fig. 2. Marginal PDFs of $x(t)$ (a) and $\dot{x}(t)$ (b) at time instants $t = 1$ s and $t = 12$ s for an SDOF hardening Duffing oscillator under Gaussian white noise excitation, as obtained via the WPI technique; comparisons with MCS data (50,000 realizations).

results (50,000 realizations) are included as well for comparison purposes. Overall, it is seen that for this specific numerical example the gain of the proposed technique in terms of computational efficiency, as compared both to the standard [11] and to the enhanced [19] implementations, is drastic. It is worth noting that the herein developed technique based on global bases can be potentially coupled with sparsity concepts and compressive sampling for further reducing the associated computational cost (see [20] for more details on sparse representations).
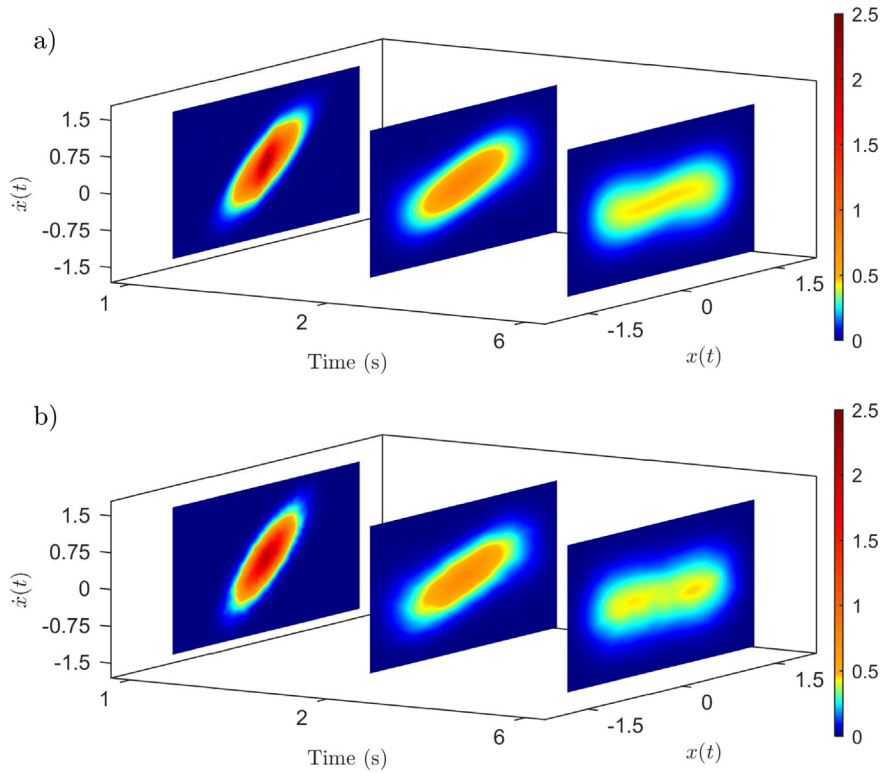
Fig. 3. Non-stationary joint PDF of $x(t)$ and $\dot{x}(t)$ at time instants $t = 1, 2$ and 6 s for an SDOF Duffing oscillator with bimodal response PDF under Gaussian white noise excitation, as obtained via the WPI technique (a); comparisons with MCS data – 50,000 realizations (b).

Fig. 4. Non-stationary marginal PDF of $x(t)$ and $\dot{x}(t)$ for an SDOF Duffing oscillator with bimodal response PDF under Gaussian white noise excitation, as obtained via the WPI technique (a and c); comparisons with MCS data – 50,000 realizations (b and d).

Fig. 5. Marginal PDFs of $x(t)$ (a) and $\dot{x}(t)$ (b) at time instants $t = 1$ s and $t = 12$ s for an SDOF Duffing oscillator with bimodal response PDF under Gaussian white noise excitation, as obtained via the WPI technique; comparisons with MCS data (50,000 realizations).

4.2. MDOF nonlinear oscillator subject to non-stationary time-modulated Gaussian white noise

In this section the efficacy of the mesh-free approximate WPI technique presented in Section 3.2 is assessed, in conjunction with a 2-DOF nonlinear dynamical system whose equation of motion is given by Eq. (2) with

$$\mathbf{M} = \begin{bmatrix} m_0 & 0 \\ 0 & m_0 \end{bmatrix}, \tag{42}$$

$$\mathbf{C} = \begin{bmatrix} 2c_0 & -c_0 \\ -c_0 & 2c_0 \end{bmatrix}, \tag{43}$$

$$\mathbf{K} = \begin{bmatrix} 2k_0 & -k_0 \\ -k_0 & 2k_0 \end{bmatrix}, \tag{44}$$

and

$$\mathbf{g}(\mathbf{x}, \dot{\mathbf{x}}) = \begin{bmatrix} \epsilon_1 k_0 x_1^3 \\ 0 \end{bmatrix} \tag{45}$$

and parameter values ($m_0 = 1; c_0 = 0.35; k_0 = 0.5; \epsilon_1 = 0.2$; and $S_0 = 0.1$). The matrix $\mathbf{D}(t)$ of Eq. (3) containing the time-modulating functions $d_1(t)$ and $d_2(t)$ is diagonal with

$$d_1(t) = d_2(t) = \gamma + \eta\left(e^{-\alpha t} - e^{-\beta t}\right) \tag{46}$$

and parameters values ($\alpha = 0.4; \beta = 1.6; \gamma = 10^{-3}$; and $\eta = 5$). The non-stationary excitation power spectrum is, thus, given as

$$\mathbf{S_w} = \begin{bmatrix} S_w(t) & 0 \\ 0 & S_w(t) \end{bmatrix}, \tag{47}$$

where $S_w(t) = S_0 d_1^2(t) = S_0 d_2^2(t)$ is shown in Fig. 6.

Considering the system initially at rest, the joint response PDF $p(\mathbf{x}, \dot{\mathbf{x}}, t)$ is sampled at $n = 60,000$ Halton points (see Section 3.2 for more details). Note that this is a rather challenging example from an approximation theory perspective due to the fact that the response PDF is non-stationary. As a result, the bounds of the effective PDF domain may vary continuously with time in an arbitrary manner. In this regard, if the bounds are pre-specified and fixed, there are measurements of the PDF whose values are effectively zero; thus, causing numerical instabilities in the approximation. This challenge can be addressed by considering "adaptive" bounds, whose time-varying values can be estimated, for instance, via a preliminary
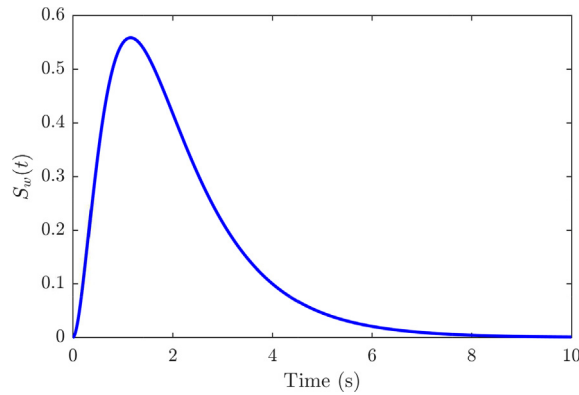
Fig. 6. Non-stationary Gaussian white noise excitation power spectrum, given by Eq. (47), where $S_w(t) = S_0 d_1^2(t) = S_0 d_2^2(t)$ and $d_1(t) = d_2(t) = \gamma + \eta(e^{-\alpha t} - e^{-\beta t})$ with parameter values ($S_0 = 0.1; \alpha = 0.4; \beta = 1.6; \gamma = 10^{-3}$; and $\eta = 5$).

MCS analysis with very few realizations (e.g., of the order of 10^2). Next, the leave-one-out cross validation follows and the set of optimal parameters (ϵ_s, ϵ_t) is determined. It is noted that, as discussed in Section 3.2.2, a 4th-degree polynomial is also added in the approximation scheme, and thus, the joint response PDF is approximated via Eq. (41) with the augmented coefficient vector determined via Eq. (40).

In Figs. 7 and 8 the joint PDFs $p(x_1, \dot{x}_1, t)$ and $p(\dot{x}_1, x_2, t)$ obtained by the approximate WPI technique based on positive definite functions are plotted, respectively. Comparisons with pertinent MCS data (50,000 realizations) demonstrate a relatively high accuracy degree. Further, as shown in Figs. 9 and 10 for the non-stationary marginal PDFs of $x_1(t)$ and $x_2(t)$, respectively, and based on comparisons with MCS data, the herein developed technique is capable of capturing accurately the evolution in time of the PDF shape and features. Furthermore, in Fig. 11 the marginal PDFs of $x_2(t)$ and $\dot{x}_2(t)$ for two arbitrary time instants are shown and compared with respective MCS-based results. In passing, note that an alternative brute-
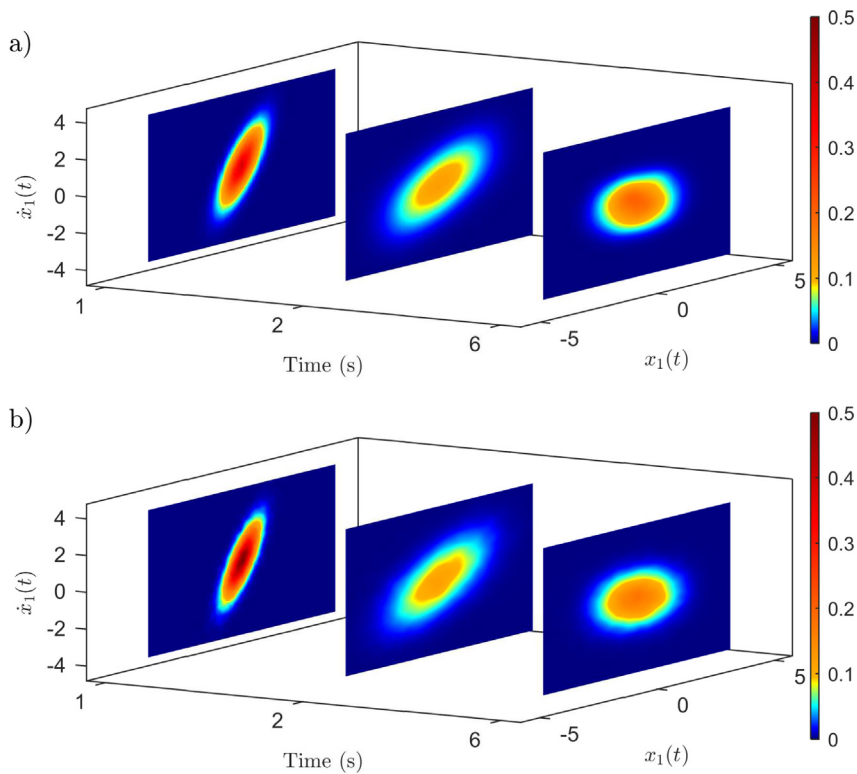
Fig. 7. Non-stationary joint PDF of $x_1(t)$ and $\dot{x}_1(t)$ at time instants $t = 1, 2$ and 6 s for a 2-DOF nonlinear system subject to time-modulated Gaussian white noise, as obtained via the WPI technique (a); comparisons with MCS data – 50,000 realizations (b).
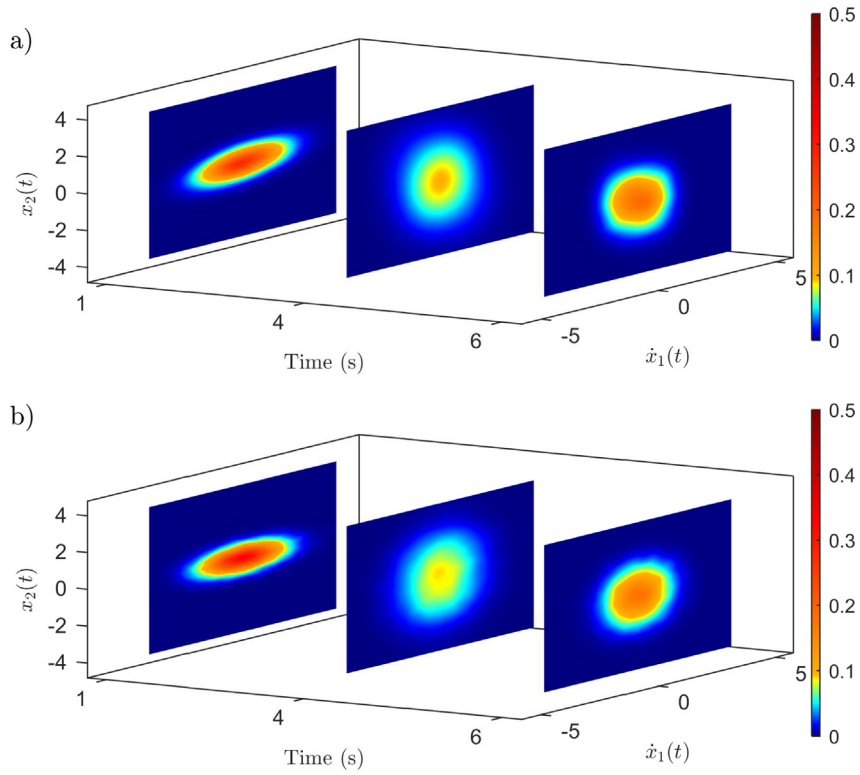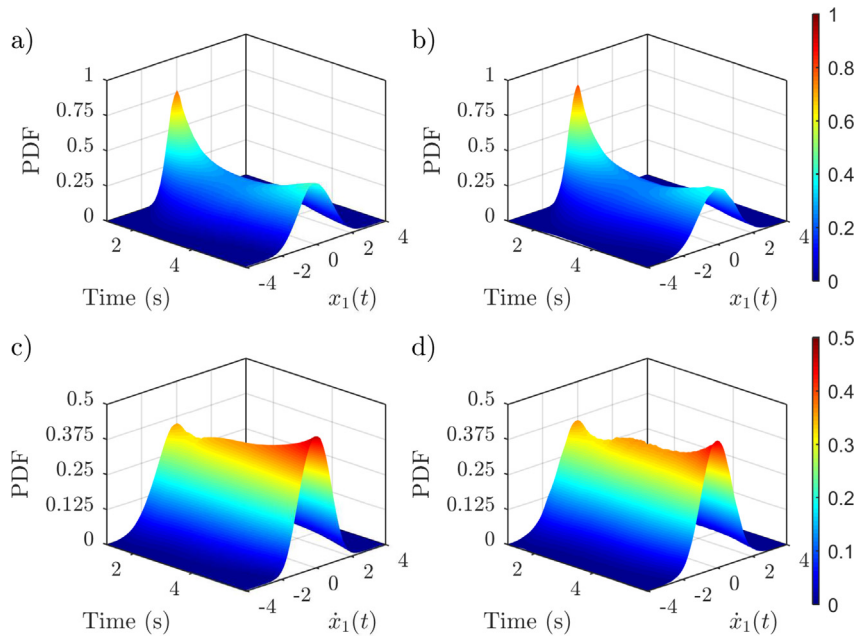
Fig. 8. Non-stationary joint PDF of $\dot{x}_1(t)$ and $x_2(t)$ at time instants $t = 1, 4$ and 6 s for a 2-DOF nonlinear system subject to time-modulated Gaussian white noise, as obtained via the WPI technique (a); comparisons with MCS data – 50,000 realizations (b).
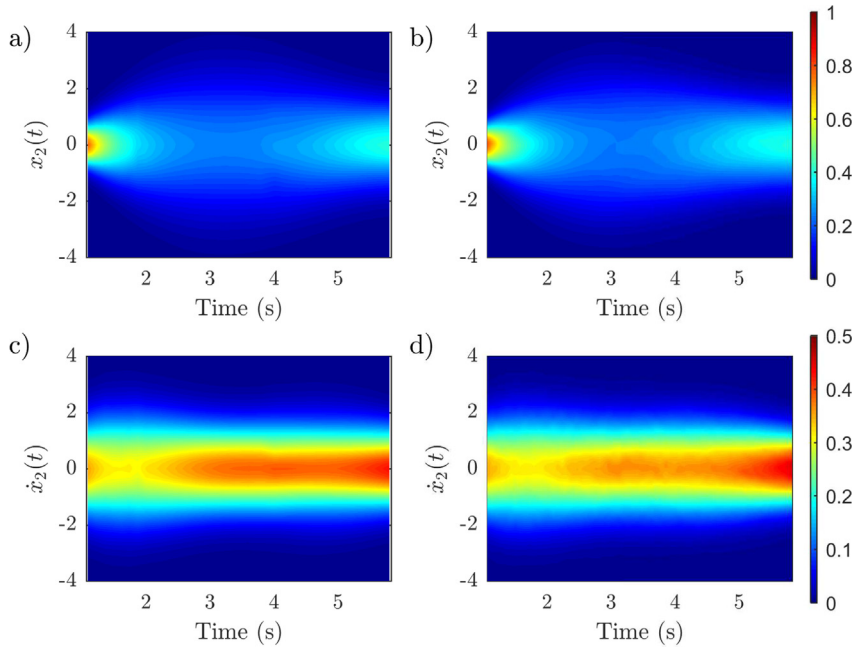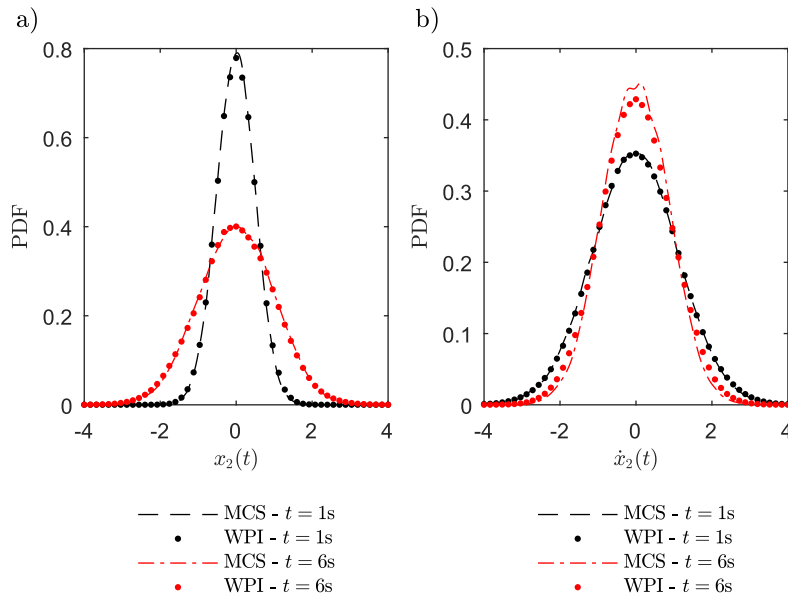

Fig. 9. Non-stationary marginal PDF of $x_1(t)$ and $\dot{x}_1(t)$ for a 2-DOF nonlinear system subject to time-modulated Gaussian white noise, as obtained via the WPI technique (a and c); comparisons with MCS data – 50,000 realizations (b and d).

Fig. 10. Non-stationary marginal PDF of $x_2(t)$ and $\dot{x}_2(t)$ for a 2-DOF nonlinear system subject to time-modulated Gaussian white noise, as obtained via the WPI technique (a and c); comparisons with MCS data – 50,000 realizations (b and d).

Fig. 11. Marginal PDFs of $x_2(t)$ (a) and $\dot{x}_2(t)$ (b) at time instants $t = 1$ s and $t = 6$ s for a 2-DOF nonlinear system subject to time-modulated Gaussian white noise, as obtained via the WPI technique (a); comparisons with MCS data – 50,000 realizations (b).

force implementation (e.g., [11,17]) and employing an expansion basis for each and every time instant independently [19] would require approximately 10^9 and 70,000 PDF measurements, respectively (assuming that the temporal dimension is, indicatively, discretized into 1,000 points).

4.3. Beam bending problem with a non-Gaussian and non-homogeneous stochastic Young's modulus

The example considered in this section serves to demonstrate that the WPI formalism delineated in Section 2 (see [17] for more details) can account not only for stochastically excited dynamical systems governed by Eq. (2), but also for certain engineering mechanics problems with stochastic media properties. In this regard, it has been shown [16,17] that a class of one-

dimensional mechanics problems with stochastic system parameters, such as the herein considered Euler-Bernoulli beam with stochastic Young's modulus, can be cast equivalently in the form of Eq. (6). Thus, the left hand-side of Eq. (6) can be used for defining an auxiliary Lagrangian function, and the WPI solution technique can be applied in a rather straightforward manner.

In this regard, a statically determinate Euler-Bernoulli beam is considered next whose response is governed by the differential equation

$$\frac{d^2}{dz^2}[E(z)I\ddot{q}(z)] = l(z) \tag{48}$$

where $E(z)$ is the Young's modulus; I is the constant cross-sectional moment of inertia; $q(z)$ is the deflection of the beam; and $l(z)$ denotes a deterministic distributed force. In this static problem the dot above a variable denotes differentiation with respect to the space variable z. Further, as explained in [16,17], Eq. (48) can be integrated twice and cast in the form

$$-\frac{M(z)}{I\ddot{q}(z)} = E(z) \tag{49}$$

where the Young's modulus is modeled as a non-Gaussian, non-white and non-homogeneous stochastic field as

$$\frac{\dot{E}(z)}{E(z)} = w(z) \tag{50}$$

with $E(0) = E_M$, and $w(z)$ is the white noise process as defined in Eq. (4). It can be readily seen that Eq. (50) represents a standard geometric Brownian motion SDE, whose space-dependent response PDF is log-normal (e.g., [82]). Combining Eq. (49) and (50) yields an equation in the form of Eq. (6); that is,

$$\frac{\dot{M}(z)}{M(z)} - \frac{q^{(3)}(z)}{\ddot{q}(z)} = w(z) \tag{51}$$

Next, the case of a cantilever beam subject to a single point moment at its free end is considered (Fig. 12). Thus, taking into account that $M(z)$ is constant along the length of the beam, i.e., $M(z) = M_0$, Eq. (51) becomes

$$-\frac{q^{(3)}(z)}{\ddot{q}(z)} = w(z) \tag{52}$$

while based on Eq. (10) the expression

$$\mathcal{L}[q, \dot{q}, \ddot{q}, q^{(3)}] = \frac{(q^{(3)}(z))^2}{4\pi S_0 (\ddot{q}(z))^2} \tag{53}$$

can be construed as the corresponding Lagrangian function. In this regard, the E-L equation becomes

$$\frac{\partial\mathcal{L}}{\partial q_c} - \frac{\partial}{\partial z}\frac{\partial\mathcal{L}}{\partial \dot{q}_c} + \frac{\partial^2}{\partial z^2}\frac{\partial\mathcal{L}}{\partial \ddot{q}_c} - \frac{\partial^3}{\partial z^3}\frac{\partial\mathcal{L}}{\partial q_c^{(3)}} = 0 \tag{54}$$

together with the initial conditions for $z_i = 0, q_c(z_i) = q_i = 0, \dot{q}_c(z_i) = \dot{q}_i = 0$ and $\ddot{q}_c(z_i) = -\frac{M_0}{E_M I}$.

Subsequently, the joint response PDF $p(q, \dot{q}, \ddot{q}, z)$ is sampled at $n = 20,000$ Halton points with bounds that vary with z. Specifically, the bounds of the response PDF space-varying effective domain are determined via a preliminary MCS with only a few realizations (see Example 4.2 for details). Next, following the evaluation of the augmented coefficient vector via Eq. (40), Eq. (41) is utilized in conjunction with an 8th-degree polynomial, and $p(q, \dot{q}, \ddot{q}, z)$ is determined. In Figs. 13 and 14 the WPI-based non-stationary (space-dependent) marginal PDFs of $q(z)$ and $\dot{q}(z)$ are shown, respectively, while MCS-based data (50,000 realizations) are also provided for comparison. Moreover, Fig. 15 shows the marginal PDFs of $q(z)$ and $\dot{q}(z)$ at $z = 0.6$, $z = 0.8$ and $z = 1$, as obtained via the herein developed technique, and includes comparisons with pertinent MCS data. It is worth mentioning that the considered beam bending problem is significantly challenging from a global approximation point of view, since the response mean varies considerably in the spatial domain; thus, rendering necessary the utilization of an adaptive with z effective PDF domain. Nevertheless, it has been shown that the WPI technique in con-
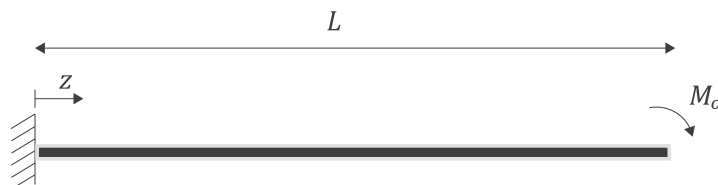

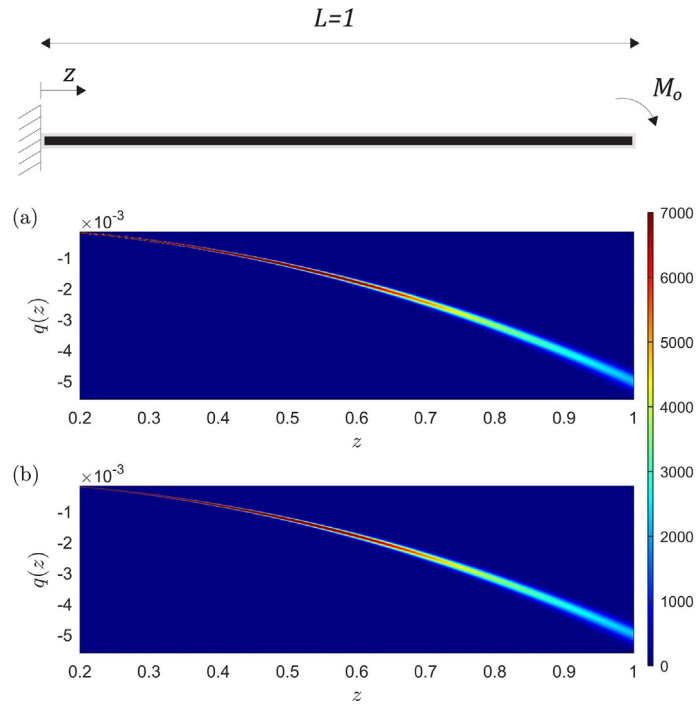**Fig. 12.** Cantilever beam subject to a single-point moment.

Fig. 13. Non-stationary (space-dependent) marginal PDF of $q(z)$ for a statically determinate beam with a non-Gaussian and non-homogeneous stochastic Young's modulus, as obtained via the WPI technique (a); comparisons with MCS data – 50,000 realizations (b).
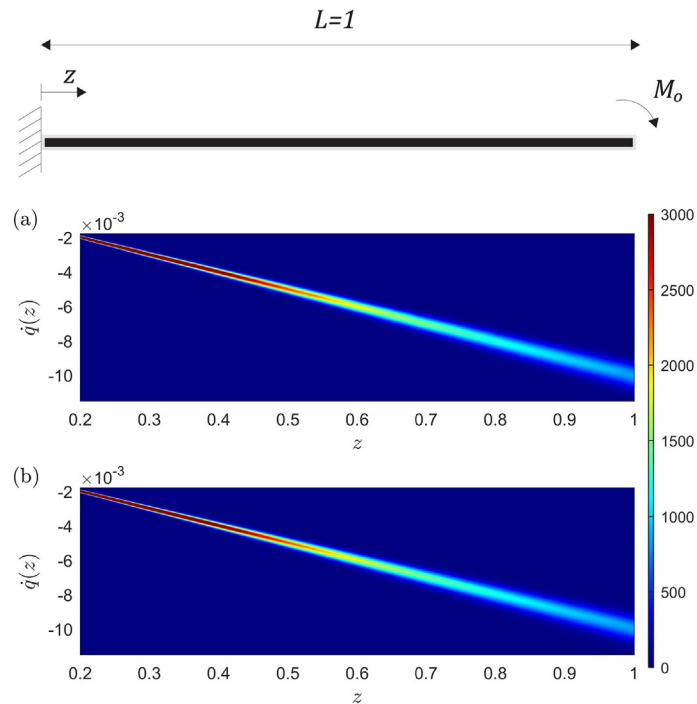

Fig. 14. Non-stationary (space-dependent) marginal PDF of $\dot{q}(z)$ for a statically determinate beam with a non-Gaussian and non-homogeneous stochastic Young's modulus, as obtained via the WPI technique (a); comparisons with MCS data – 50,000 realizations (b).

junction with positive definite functions for approximating the joint response PDF yields accurate results at a relatively low computational cost. In this regard, note for comparison purposes that alternative implementations, such as the brute-force scheme delineated in Section 2.2, would require a several orders of magnitude higher number of PDF measurements. Further,
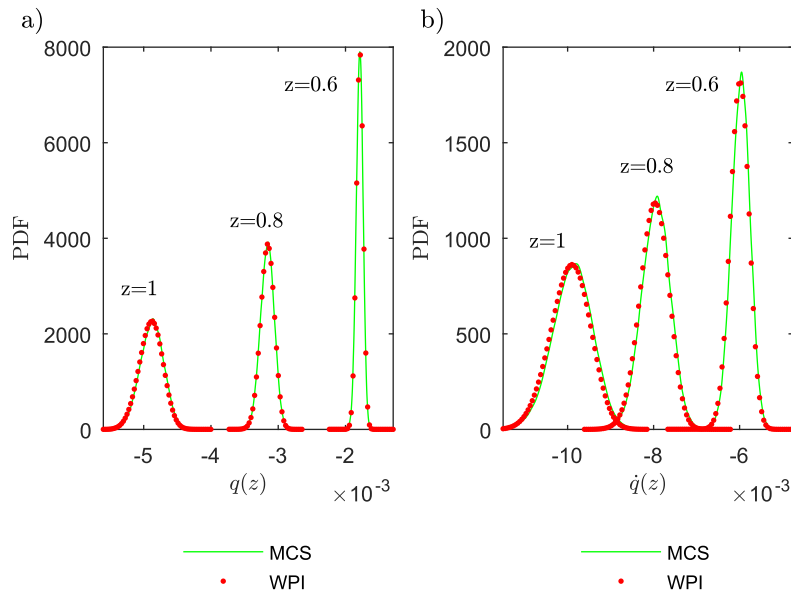
Fig. 15. Marginal PDFs of $q(z)$ (a) and $\dot{q}(z)$ (b) at $z = 0.6$, $z = 0.8$ and $z = 1$ for a statically determinate beam with a non-Gaussian and non-homogeneous stochastic Young's modulus, as obtained via the WPI technique; comparisons with MCS data (50,000 realizations).

a direct comparison in terms of cost with the enhanced implementation in [19] is not possible as the 4th-order polynomial employed in [19] would be, most likely, an inappropriate choice for approximating the joint response $p(q, \dot{q}, \ddot{q}, z)$.

5. Concluding remarks

In this paper, the WPI technique has been generalized and enhanced for determining directly, and in a computationally efficient manner, the complete time-dependent non-stationary response PDF of stochastically excited nonlinear multi-degree-of-freedom dynamical systems. This has been done, first, by constructing multi-dimensional (time-dependent) global bases for approximating the non-stationary joint response PDF, and second, by exploiting the localization capabilities of the WPI technique for determining PDF points in the joint space-time domain. These points have been used for evaluating the expansion coefficients at a relatively low computational cost. Specifically, two distinct expansions have been constructed: the first is based on Kronecker products of bases (e.g., wavelets), while the second employs positive definite functions. Although the performance of the expansions in approximating the response PDF is, in general, problem-dependent, it can be argued that positive definite functions appear more versatile and suitable for handling higher-dimensional problems, whereas Kronecker products perform better for lower-dimensional problems, especially when some information regarding the PDF is available a priori.

Several numerical examples pertaining to both single- and multi-degree-of-freedom nonlinear dynamical systems subject to non-stationary excitations have been considered for assessing the reliability of the technique. Further, to illustrate that the technique can account also for certain engineering mechanics problems with stochastic media properties, a bending beam with a non-Gaussian and non-homogeneous Young's modulus has been included in the numerical examples as well. The latter example has also been found to be significantly challenging from a global approximation perspective, since the response PDF effective domain varies considerably along the spatial dimension. Nevertheless, this challenge can be addressed by utilizing adaptive PDF domain bounds. Comparisons with pertinent MCS data have demonstrated a relatively high accuracy degree for all the considered examples.

Finally, although the related computational cost is, in general, problem-dependent, it has been shown that in most examples considered herein the computational efficiency exhibited by the developed technique is significant. Specifically, compared both to a brute-force numerical implementation (see Section 2.2) and to employing an expansion basis for each and every time instant independently [19], the gain in terms of computational cost of the herein proposed WPI technique enhancement is notable, measured even at several orders of magnitude for some cases. Future work relates to coupling the proposed WPI technique with sparse representations and compressive sampling [20] for further reducing the computational cost.

Acknowledgment

References

[1] M. Grigoriu, Stochastic Calculus: Applications in Science and Engineering, Birkhäuser, Basel, 2002.
[2] E. Vanmarcke, Random Fields: Analysis and Synthesis, World Scientific, 2010.
[3] T. Soong, M. Grigoriu, Random Vibration of Mechanical and Structural Systems, Prentice Hall, New Jersey, 1993.
[4] J.B. Roberts, P.D. Spanos, Random Vibration and Statistical Linearization, Dover, New York, 2003.
[5] J. Li, J. Chen, Stochastic Dynamics of Structures, Wiley, New York, 2009.
[6] R.G. Ghanem, P.D. Spanos, Stochastic Finite Elements: A Spectral Approach, Dover, New York, 2003.
[7] G. Stefanou, The stochastic finite element method: past, present and future, Comput. Methods Appl. Mech. Eng. 198 (9–12) (2009) 1031–1051.
[8] K. Teferra, G. Deodatis, Variability response functions for beams with nonlinear constitutive laws, Probab. Eng. Mech. 29 (2012) 139–148.
[9] A. Burlon, G. Failla, F. Arena, Exact stochastic analysis of coupled bending–torsion beams with in-span supports and masses, Probab. Eng. Mech. 54 (2018) 53–64.
[10] I.A. Kougioumtzoglou, P.D. Spanos, An analytical wiener path integral technique for non-stationary response determination of nonlinear oscillators, Probab. Eng. Mech. 28 (2012) 125–131.
[11] I.A. Kougioumtzoglou, P.D. Spanos, Nonstationary stochastic response determination of nonlinear systems: a Wiener path integral formalism, J. Eng. Mech. 140 (9) (2014) 04014064.
[12] N. Wiener, The average of an analytic functional and the Brownian movement, Proc. Nat. Acad. Sci. 7 (10) (1921) 294–298.
[13] R.P. Feynman, Space-time approach to non-relativistic quantum mechanics, Rev. Mod. Phys. 20 (2) (1948) 367.
[14] M. Chaichian, A. Demichev, Path Integrals in Physics: Stochastic Processes and Quantum Mechanics, Institute of Physics Publishing, Bristol, U.K., 2001.
[15] A. Di Matteo, I.A. Kougioumtzoglou, A. Pirrotta, P.D. Spanos, M. Di Paola, Stochastic response determination of nonlinear oscillators with fractional derivatives elements via the Wiener Path Integral, Probab. Eng. Mech. 38 (2014) 127–135.
[16] I.A. Kougioumtzoglou, A wiener path integral solution treatment and effective material properties of a class of one-dimensional stochastic mechanics problems, J. Eng. Mech. 143 (6) (2017) 04017014.
[17] A.F. Psaros, O. Brudastova, G. Malara, I.A. Kougioumtzoglou, Wiener Path Integral based response determination of nonlinear systems subject to non-white, non-Gaussian, and non-stationary stochastic excitation, J. Sound Vib. 433 (2018) 314–333.
[18] I. Petromichelakis, A.F. Psaros, I.A. Kougioumtzoglou, Stochastic response determination and optimization of a class of nonlinear electromechanical energy harvesters: a Wiener path integral approach, Probab. Eng. Mech. 53 (2018) 116–125.
[19] I.A. Kougioumtzoglou, A. Di Matteo, P.D. Spanos, A. Pirrotta, M. Di Paola, An efficient Wiener Path Integral technique formulation for stochastic response determination of nonlinear MDOF systems, J. Appl. Mech. 82 (10) (2015) 101005.
[20] A.F. Psaros, I.A. Kougioumtzoglou, I. Petromichelakis, Sparse representations and compressive sampling for enhancing the computational efficiency of the Wiener path integral technique, Mech. Syst. Signal Process. 111 (2018) 87–101.
[21] I.A. Kougioumtzoglou, P.D. Spanos, An approximate approach for nonlinear system response determination under evolutionary stochastic excitation, Curr. Sci. (2009) 1203–1211.
[22] V. John, I. Angelov, A. Öncül, D. Thévenin, Techniques for the reconstruction of a distribution from a finite number of its moments, Chem. Eng. Sci. 62 (11) (2007) 2890–2904.
[23] P. Gavriliadis, G. Athanassoulis, The truncated Stieltjes moment problem solved by using kernel density functions, J. Comput. Appl. Math. 236 (17) (2012) 4193–4213.
[24] C. Soize, The Fokker-Planck equation for stochastic dynamical systems and its explicit steady state solutions, vol. 17, World Scientific, 1994.
[25] J.F. Dunne, M. Ghanbari, Extreme-value prediction for non-linear stochastic oscillators via numerical solutions of the stationary FPK equation, J. Sound Vib. 206 (5) (1997) 697–724.
[26] T.P. Sapsis, G.A. Athanassoulis, New partial differential equations governing the joint, response–excitation, probability distributions of nonlinear systems, under general stochastic excitation, Probab. Eng. Mech. 23 (2–3) (2008) 289–306.
[27] G. Muscolino, G. Ricciardi, M. Vasta, Stationary and non-stationary probability density function for non-linear oscillators, Int. J. Non-Linear Mech. 32 (6) (1997) 1051–1064.
[28] S. McWilliam, D. Knappett, C. Fox, Numerical solution of the stationary FPK equation using Shannon wavelets, J. Sound Vib. 232 (2) (2000) 405–430.
[29] M. Di Paola, A. Sofi, Approximate solution of the Fokker–Planck–Kolmogorov equation, Probab. Eng. Mech. 17 (4) (2002) 369–384.
[30] D.H. Hawes, R.S. Langley, Numerical methods for calculating the response of a deterministic and stochastically excited Duffing oscillator, Proc. Inst. Mech. Eng., Part C: J. Mech. Eng. Sci. 230 (6) (2016) 888–899.
[31] S.H. Crandall, Non-Gaussian closure for random vibration of non-linear oscillators, Int. J. Non-Linear Mech. 15 (4–5) (1980) 303–313.
[32] Q. Liu, H. Davies, The non-stationary response probability density functions of non-linearly damped oscillators subjected to white noise excitations, J. Sound Vib. 139 (3) (1990) 425–435.
[33] G.-K. Er, An improved closure method for analysis of nonlinear stochastic systems, Nonlinear Dyn. 17 (3) (1998) 285–297.
[34] H.K. Joo, T.P. Sapsis, A moment-equation-copula-closure method for nonlinear vibrational systems subjected to correlated noise, Probab. Eng. Mech. 46 (2016) 120–132.
[35] S.-S. Guo, Nonstationary solutions of nonlinear dynamical systems excited by Gaussian white noise, Nonlinear Dyn. 92 (2) (2018) 613–626.
[36] M. Kumar, S. Chakravorty, J.L. Junkins, A semianalytic meshless approach to the transient Fokker-Planck equation, Probab. Eng. Mech. 25 (3) (2010) 323–331.
[37] J. Náprstek, R. Král, Finite element method analysis of Fokker-Plank equation in stationary and evolutionary versions, Adv. Eng. Softw. 72 (2014) 28–38.
[38] A. Naess, J. Johnsen, Response statistics of nonlinear, compliant offshore structures by the path integral solution method, Probab. Eng. Mech. 8 (2) (1993) 91–106.
[39] A. Naess, V. Moe, Efficient path integration methods for nonlinear dynamic systems, Probab. Eng. Mech. 15 (2) (2000) 221–231.
[40] W.-X. Xie, W. Xu, L. Cai, Numerical meshfree path integration method for non-linear dynamic systems, Appl. Math. Comput. 197 (1) (2008) 426–434.
[41] S. Narayanan, P. Kumar, Numerical solutions of Fokker-Planck equation of nonlinear systems subjected to random and harmonic excitations, Probab. Eng. Mech. 27 (1) (2012) 35–46.
[42] K. Sobczyk, J. Trcebicki, Approximate probability distributions for stochastic systems: maximum entropy method, Comput. Methods Appl. Mech. Eng. 168 (1–4) (1999) 91–111.
[43] A. Batou, C. Soize, Calculation of Lagrange multipliers in the construction of maximum entropy distributions in high stochastic dimension, SIAM/ASA J. Uncertainty Quantif. 1 (1) (2013) 431–451.
[44] X. Zhang, Y. Zhang, M. Pandey, Y. Zhao, Probability density function for stochastic response of non-linear oscillation system under random excitation, Int. J. Non-Linear Mech. 45 (8) (2010) 800–808.
[45] Y. Hasegawa, Variational superposed Gaussian approximation for time-dependent solutions of Langevin equations, Phys. Rev. E 91 (4) (2015) 042912.
[46] S. Kazem, J. Rad, K. Parand, Radial basis functions methods for solving Fokker-Planck equation, Eng. Anal. Boundary Elem. 36 (2) (2012) 181–189.
[47] M. Dehghan, V. Mohammadi, The numerical solution of Fokker-Planck equation with radial basis functions (RBFs) based on the meshless technique of Kansa' s approach and Galerkin method, Eng. Anal. Boundary Elem. 47 (2014) 38–63.
[48] G.M. Ewing, Calculus of Variations with Applications, Dover, New York, 1985.
[49] M.F. Duarte, R.G. Baraniuk, Kronecker compressive sensing, IEEE Trans. Image Process. 21 (2) (2012) 494–504.
[50] G.E. Fasshauer, Positive definite kernels: past, present and future, Dolomite Res. Notes Approx. 4 (2011) 21–63.
[51] C.F. Caiafa, A. Cichocki, Computing sparse representations of multidimensional signals using Kronecker bases, Neural Comput. 25 (1) (2013) 186–220.
[52] M. Cossalter, G. Valenzise, M. Tagliasacchi, S. Tubaro, Joint compressive video coding and analysis, IEEE Trans. Multimedia 12 (3) (2010) 168–183.

[53] C.F. Van Loan, N. Pitsianis, Approximation with Kronecker products, in: Linear algebra for large scale and real-time applications, Springer, 1993, pp. 293–314.
[54] F. Lamping, J.-M. Peña, T. Sauer, Spline approximation, Kronecker products and multilinear forms, Numer. Linear Algebra Appl. 23 (3) (2016) 535–557.
[55] S. Mallat, A Wavelet Tour of Signal Processing: The Sparse Way, Academic Press, 2008.
[56] D.E. Newland, Harmonic and musical wavelets, Proc. R. Soc. Lond. A 444 (1922) (1994) 605–620.
[57] I.A. Kougioumtzoglou, P.D. Spanos, An identification approach for linear and nonlinear time-variant structural systems via harmonic wavelets, Mech. Syst. Signal Process. 37 (1–2) (2013) 338–352.
[58] P.D. Spanos, F. Kong, J. Li, I.A. Kougioumtzoglou, Harmonic wavelets based excitation–response relationships for linear systems: a critical perspective, Probab. Eng. Mech. 44 (2016) 163–173.
[59] S. Mann, S. Haykin, The chirplet transform: physical considerations, IEEE Trans. Signal Process. 43 (11) (1995) 2745–2761.
[60] P.D. Spanos, G. Failla, Wavelets: theoretical concepts and vibrations related applications, Shock Vibr. Dig. 37 (5) (2005) 359.
[61] P.J. Olver, On multivariate interpolation, Stud. Appl. Math. 116 (2) (2006) 201–240.
[62] M. Van Barel, M. Humet, L. Sorber, Approximating optimal point configurations for multivariate polynomial interpolation, Electron. Trans. Numer. Anal. 42 (2014) 41–63.
[63] G.E. Fasshauer, Meshfree Approximation Methods with Matlab:(With CD-ROM), vol. 6, World Scientific Publishing Company, 2007.
[64] D. Braess, Nonlinear Approximation Theory, vol. 7, Springer Science & Business Media, 2012.
[65] G. Fasshauer, M. McCourt, Kernel-Based Approximation Methods Using Matlab, World Scientific Publishing Company, 2015, vol. 19.
[66] C.A. Micchelli, Interpolation of scattered data: distance matrices and conditionally positive definite functions, in: Approximation Theory and Spline Functions, Springer, 1984, pp. 143–145.
[67] R. Yokota, L.A. Barba, M.G. Knepley, PetRBF-A parallel O(N) algorithm for radial basis function interpolation with Gaussians, Comput. Methods Appl. Mech. Eng. 199 (25–28) (2010) 1793–1804.
[68] B. Fornberg, N. Flyer, A Primer on Radial Basis Functions with Applications to the Geosciences, SIAM, 2015.
[69] B. Niu, Monte Carlo simulation of infinite-dimensional integrals, Illinois Institute of Technology (2011) (Ph.D. thesis).
[70] R. Schaback, H. Wendland, Kernel techniques: from machine learning to meshless methods, Acta Numerica 15 (2006) 543–639.
[71] M.D. Buhmann, Radial Basis Functions: Theory and Implementations, vol. 12, Cambridge University Press, 2003.
[72] R. Opfer, Multiscale kernels, Adv. Comput. Math. 25 (4) (2006) 357–380.
[73] J.H. Halton, On the efficiency of certain quasi-random sequences of points in evaluating multi-dimensional integrals, Numer. Math. 2 (1) (1960) 84–90.
[74] P. Bratley, B.L. Fox, H. Niederreiter, Implementation and tests of low-discrepancy sequences, ACM Trans. Model. Comput. Simul. (TOMACS) 2 (3) (1992) 195–213.
[75] S. De Marchi, R. Schaback, H. Wendland, Near-optimal data-independent point locations for radial basis function interpolation, Adv. Comput. Math. 23 (3) (2005) 317–330.
[76] O.C. Zienkiewicz, R.L. Taylor, The Finite Element Method for Solid and Structural Mechanics, Elsevier, 2005.
[77] H. Wendland, Scattered Data Approximation, vol. 17, Cambridge University Press, 2004.
[78] S. De Marchi, R. Schaback, Stability of kernel-based interpolation, Adv. Comput. Math. 32 (2) (2010) 155–161.
[79] M. Mongillo, Choosing basis functions and shape parameters for radial basis function methods, SIAM Undergraduate Research Online 4 (2011) 190–209.
[80] S. Rippa, An algorithm for selecting a good value for the parameter c in radial basis function interpolation, Adv. Comput. Math. 11 (2–3) (1999) 193–210.
[81] M. Pazouki, R. Schaback, Bases for kernel-based spaces, J. Comput. Appl. Math. 236 (4) (2011) 575–588.
[82] B. Øksendal, Stochastic Differential Equations, Springer-Verlag, Berlin, 2003.